FEATURE ARTICLE

# Solvation and Ionization Stages of HCl on Ice Nanocrystals

**Victoria Buch**[†]

*The Fritz Haber Institute for Molecular Dynamics, Hebrew University, Jerusalem 91904, Israel*

**Joanna Sadlej**[‡]

*Department of Chemistry, University of Warsaw, Pasteura 1, 02-093 Warsaw, Polandand Drug Institute, Chelmska 30/34, 00-725 Warsaw, Poland*

**Nevin Aytemiz-Uras**[§]

*Department of Chemistry, Suleyman Demirel University, Isparta, Turkey*

**J. Paul Devlin***

*Department of Chemistry, Oklahoma State University, Stillwater, Oklahoma 74078*

*Received: July 1, 2002*

The study focuses on acid adsorption on cold ice particle surfaces. The investigation encompasses HCl, DCl, and HBr adsorbate spectroscopy, Monte Carlo simulations of molecular HCl adsorbate on a model ice particle, and ab initio studies of HCl solvation and ionization in mixed acid−water clusters. It is shown that ice nanocrystal surfaces offer a range of adsorption sites, in which HCl freezes in different recognizable solvation stages. These stages were identified spectroscopically and assigned, with the help of calculations, to weakly and strongly stretched HCl molecules, and to Zundel and hydronium ions that are products of proton transfer. At moderate submonolayer coverages in the 50−60 K range, the acid adsorbate is predominantly molecular. Heating promotes formation of contact hydronium − chloride ion pairs. Near 90 K, an ionization burst is observed, resulting in an ionic surface hydrate layer rich in Zundel cations.

## 1. Introduction

Ionization of hydrochloric acid, $HCl + H_2O \rightarrow H_3O^+ + Cl^-$, is a very basic reaction in chemistry. It is driven by ion solvation in water; i.e., the ions form strong hydrogen bonds with the solvent, and the formation of the solvation shell renders the resulting reaction exothermic and thermodynamically favorable. Recently, there has been enhanced interest in the acid ionization reaction on the ice surface, in connection with the ozone hole formation. This is because HCl adsorption and ionization on stratospheric ice particles was proposed as one of the important steps in the reaction chain leading to ozone destruction.[1−3] The HCl solvation mechanism also attracted considerable attention in the context of the minimum extent of solvation necessary for acid ionization, and the ability of confined-water media such as clusters and ice surfaces to induce the ionization (see, e.g., refs 4−47). The latter issue is addressed here for acid adsorbate on cold ice nanocrystal surfaces; preliminary results were published.[48] Our focus is on solvation and ionization stages of acid adsorbate under "quasi-static" conditions of essentially zero vapor pressure ($T \leq 110$ K). The tools of this investigation are FTIR spectroscopy, Monte Carlo simulation, and ab initio calculations.

Past ab initio studies of HCl and HBr solvation focused on mixed water−acid clusters containing several water molecules.[5−13] It was shown that a minimum of four water molecules is needed for stable ionic structures. A similar conclusion was reached from matrix isolation spectroscopy of the pertinent clusters;[4] however, in that study assignment of bands to different clusters has been problematic except for the smallest sizes. For the HCl and HBr adsorbate−ice-surface system, both experimental (e.g., refs 14−33) and theoretical (e.g., refs 34−47) studies have been pursued extensively.

The extent of acid ionization on the ice surface attracted considerable theoretical attention. Gertner and Hynes proposed an HCl ionization mechanism under stratospheric conditions, via incorporation into a continuously regenerated ice particle surface.[36,39] The extent of acid solvation during adsorption *on* the ice surface (rather than during incorporation into the ice lattice) was addressed by a number of studies, with different results. *Molecular* adsorption was obtained in several electronic structure studies, in which relaxation of the system was restricted by a finite size and periodic boundaries, zero surface temperature, and/or a limited number of relaxing coordinates.[38,40,45]

* Corresponding author. E-mail: devlin@okstate.edu.
[†] E-mail: viki@fh.huji.ac.il.
[‡] E-mail: sadlej@joanna.chem.uw.edu.pl.
[§] E-mail: aytemiz@fef.sdu.edu.tr.

10.1021/jp021539h CCC: $22.00 
Published on Web 09/25/2002

Molecular adsorption was also investigated in simulations employing empirical (un-ionizing) potentials.[34,37,41,43] The above studies resulted in adsorption energies in the range 5−11 kcal/mol for un-ionized HCl adsorbate on a crystalline ice surface. Clary and Wang suggested an important role of surface defects in extending the lifetime of physisorbed molecules under stratospheric conditions, to allow for encapsulation in the ice surface and ionization.[37] Cassasa proposed that HCl may be able to ionize after displacing water from the surface.[42] On the other hand, nearly barrierless HCl ionization was obtained in a QM/MM molecular dynamics simulation of HCl collisions with a crystal ice surface by Svanberg et al., employing the PM3 semiempirical molecular orbital scheme.[44] The ionization depended on HCl sticking to a commonly available site on a basal plane, in which one dangling-O (d-O) and two dangling-H (d-H)-atoms of ice are available for adsorbate bonding. (The notation d-O/d-H is used for dangling water atoms, with unsaturated hydrogen bond coordination with respect to other $H_2O$.) A facile transition was proposed to occur to such locations from less favorable binding sites. A DFT-based on-the-flight simulation of Mantz et al. in the 150−230 K range resulted in similarly efficient ionization on ice-surface regions rich in d-H.[46]

A variety of experimental techniques have been applied to investigate the acid−surface interaction, and the extent of ionization. Briefly, experimental evidence points toward metastable *molecular* HCl at low temperatures of tens of degrees Kelvin, and a transition to an ionized adsorbate layer as the temperature is increased toward 100 K; however, the results reported by different groups are not entirely consistent. Spectroscopic features due to molecular HCl (∼2500 $cm^{-1}$), DCl (∼1820 $cm^{-1}$), and HBr (∼2220 $cm^{-1}$) were identified by Delzeit et al. on the amorphous ice surface in the 15−60 K range.[15] The molecular bands were shown to persist up to 125 K on ice nanoparticles at submonolayer coverages.[24] Bands due to protonated water (a product of acid ionization) were observed as well on ice nanoparticles at 85 K,[15] and on ice films above 80 K.[20,33]

Kang et al.[28] probed the extent of HCl ionization on nonporous amorphous ice films by $Cs^+$ ion scattering; molecular HCl was detected from a reactive ion scattering product $CsHCl^+$, and ionized acid, from the protonated water SIMS signal. The ionization extent was shown to increase with temperature. Predominantly molecular HCl was detected below 70 K, comparable amounts of ionic and molecular species were obtained in the 90−120 K range, and at 140 K the ionization was complete. On the other hand, complete ionization of HCl on ice films was concluded from a SIMS study by Donsig and Vickerman[23] (above 90 K), and from a spectroscopic investigation by Banham et al.[20] (above 80 K). The apparent contradiction may be due to sensitivity of ionization to HCl coverage; see section 4.

A number of molecular-beam scattering studies demonstrated efficient trapping of HCl on the ice surface.[17,26,27] Isacson and Sitz employed pulsed-beam and mass-spectrometric techniques to study HCl adsorption on thin ice films in the 100−170 K range.[26] Analysis of the data in the 100−125 K range suggested two HCl components; the first was characterized by a desorption energy of 6.7 kcal/mol, in the range proposed for molecular HCl. The second component, presumably ionized and hydrated HCl, was "lost" on the surface in a process having an activation energy of 5.0 kcal/mol. The apparent molecular-beam reflectivity decreased substantially between 126 and 140 K, in qualitative accord with the results of Kang et al.[28] At 80−120 K, Haq et al. obtained saturation of HCl uptake on ice films of one HCl molecule for each surface $H_2O$.[32]

At higher temperatures (which are beyond the scope of the present study), the acid−ice system is very dynamic. A number of studies demonstrated penetration of HCl adsorbate into the ice lattice to form ionic hydrates, occurring upon extended exposure of the surface to HCl above 110 K (see, e.g., refs 21, 25, 30, 32, and 33). At temperatures approaching stratospheric ones, experimental studies required finite gas pressures to stabilize the solid, and the HCl−ice interaction occurred under conditions of constant evaporation and condensation.[22,25,27]

Due to its complexity, the acid adsorbate−ice-surface system is still far from being well understood. Considerable discussion is associated with a number of topics, such as the onset temperature and the extent of adsorbate penetration,[17,19,30,32] the acid-to-water ratio in hydrate products formed under different conditions,[19,20,22,32] and the influence of surface morphology on the HCl−ice interaction.[19,25,26,29,32] The experimentally derived binding energies and enthalpies of HCl on ice range from 6 to ∼18 kcal/mol;[19,26,27,49,50] this large spread of values is not surprising considering the varying extents of ionization and penetration at different experimental coverages and temperatures.

The aim of this study is to advance molecular level understanding of the acid−ice nanoparticle interaction in the low temperature regime, below the penetration threshold. The critical measurements are the FTIR difference spectra between HCl-covered nanocrystals, and bare nanocrystals prepared under similar conditions. The difference method eliminates the interior ice bands so that spectral features due to adsorbate can be examined. The resulting broad bands evolve as a function of temperature due to a transition from a predominantly molecular to a predominantly ionic surface layer.

Atomic level understanding of this system poses a serious theoretical challenge. Simulations are difficult due to lack of empirical potentials that include both an accurate description of proton transfer from acid to water, and between water molecules. Here we employ Monte Carlo (MC) simulations of *molecular* HCl on an ice particle, aiming to obtain information on the molecular adsorbate layer at 50 K. Furthermore, ab initio techniques are applied to study cluster models, in which HCl can both stretch and ionize. However, as shown below a fairly high level of ab initio calculation is necessary to describe HCl solvation, restricting the size of feasible $(H_2O)_n\cdots(HCl)_m$ models to $n \leq 7$, $m \leq 2$.

Interpretation of the spectra for this quantum-mechanical and very anharmonic system also poses considerable difficulties. The most complex issue is proton dynamics. Protonated water appears in two limiting forms: hydronium $H_3O^+$ and Zundel $H_5O_2^+$. (In the Zundel form the proton is shared by two water molecules: $H_2O\cdots H^+\cdots OH_2$.) These distinct forms were identified in crystalline HCl hydrates.[58] In aqueous solution, in which the proton undergoes diffusion, continuous interconversion occurs between the two forms.[51−55] In amorphous solids such as the ionized adsorbate layer, a frozen continuum of configurations intermediate between hydronium and Zundel is likely to be present. Moreover ab initio calculations (see section 2.2) suggest facile transitions between distinct bonding configurations separated by low barriers. Thus structural changes may be included already within the range of zero-point motion, or thermal excitations at low *T*. A path integral study of a solvated proton in a liquid in fact showed quantum delocalization of a proton over both a Zundel and a hydronium structure.[56]

The extreme anharmonicity of the acid−surface system is evidenced by the so-called "Zundel effect", i.e., an intense *continuum* absorption underlying the spectral bands;[57] this feature is observed for both liquid and solid systems rich in Zundel ions. The effect is due to continuous modulation of the proton potential well by the O···O stretch, other local motions, and fluctuations of the electric field. Thus the proton potential extends from a single well for short O···O distances, to either symmetric or asymmetric double wells.[51,52,54,55] The proton motion modulates in turn the local intermolecular interactions; e.g., $H^+$ approach to one of the water molecules affects its stretch and bending force constants.

We did not attempt as yet accurate calculation of spectra for this complex anharmonic system. Assignment of the measured spectra is aided by ab initio normal-mode analysis of cluster models, which provides information on the not-very-anharmonic motions. Comparison to amorphous-hydrate spectra was also useful because the structures of crystal analogues are known.[58] Although complete understanding was not attained, these limited tools provide considerable qualitative insight to the structural evolution of the HCl−ice system as a function of temperature.

In section 2, the computations are described. Section 3 describes the experimental setup. The main experimental results of this study, the acid adsorbate spectra as a function of temperature, are reported in section 4; the computational results of section 2 are used for the interpretation. Section 5 summarizes the results. Appendix I provides auxiliary results for the spectra of ionic hydrate and deuterate films. Following the accepted usage,[59] the term "oxonium ions" is used throughout as a generic name for all forms of protonated water, including Zundel and hydronium ions.

## 2. Computations

**2.1. Monte Carlo Simulations.** In these calculations, a fixed amount of HCl molecules (18 or 79) was deposited on an ice particle containing 293 water molecules (Figure 1). The system was simulated using classical canonical Monte Carlo at 50 K.[60]

*2.1.1. Computational Details.* The computational MC procedure is similar to the one used in our past simulations of $NH_3$ adsorption on ice.[61] A brief summary is given below with further details found in the Supporting Information and in refs 61 and 69.

The Ice-Particle Model. At low temperatures ice particles tend to freeze to a cubic ice form (ice Ic).[62−65] The O-atoms form a periodic pattern; however, water orientations are quasi-random within the constraints of the nearly perfect tetrahedral bonding geometry.[62,63] The properties of ice Ic are very similar to those of the common hexagonal ice Ih form, which is likewise orientationally disordered. Ice nanoparticle structure and spectroscopy were pursued by us in the past.[66−70] It was shown that ice nanoparticles are characterized by a crystalline interior and a disordered surface. The surface structure is dictated by the need to terminate the crystalline interior in an approximately spherical geometry. Hydrogen bond flexibility is sufficient for most surface $H_2O$ molecules to acquire four hydrogen bonds, although with a coordination shell strongly distorted from tetrahedral symmetry. (Scarcity of under-coordinated molecules makes the surface a poor solvating medium; see below.) The ice particle model $(H_2O)_{293}$ (Figure 1) used in the calculation was constructed as described in ref 61. The experiments employed much larger particles of average diameter ∼12 nm, with tens of thousands of water molecules. However, even at the size of a few hundred molecules, we obtained the basic structural pattern of a nearly crystalline core and a disordered surface; see Figure 1 and ref 69.

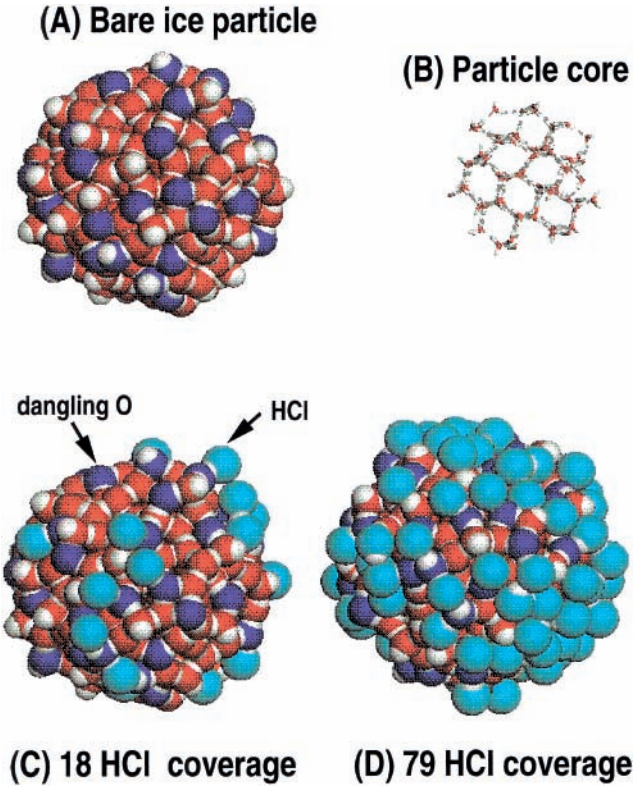


**Figure 1.** (A) $(H_2O)_{293}$ bare ice-particle model. Dangling-O-atoms are dark blue. (B) Hydrogen bond network in the core of the ice particle; crystalline order is largely retained in the interior. (C, D) Simulation snapshots with 18 and 79 HCl molecules.

The Potential. A nonpolarizable potential surface (PES) was employed with the monomers assumed rigid. The TIP4 potential was used for water−water interactions.[71] For HCl···HCl interaction, the potential of ref 72 was adopted. The HCl···$H_2O$ potential was constructed by applying Lorentz−Berthelot mixing rules to the $H_2O$···$H_2O$ and HCl···HCl potentials,[71,73] which employ a single Lennard-Jones center on the heavy atoms, plus point charges. The same point charges were adopted for the HCl···$H_2O$ potential, together with Lennard-Jones parameters $\sigma = 3.3$ Å and $\epsilon = 0.31$ kcal/mol; the parameters correspond to slightly readjusted values obtained by using the well-known mixing rules. The energy minimum in the configuration in which HCl is collinear with the water bisector corresponds to a Cl··· O distance of 3.12 Å and a well depth of 4.4 kcal/mol. For comparison, the corresponding ab initio values reported for the HCl···$H_2O$ dimer are in the range 3.12−3.22 Å and 4.0−5.5 kcal/mol.[5,11,45,74] As seen in Figure 2, for these potentials the $H_2O$···$H_2O$ bond in the optimal orientation is stronger than the $H_2O$···HCl bond, and HCl···HCl and HCl···HOH bonds are much weaker. (The weakness of the HCl···HOH interaction was also noted in an ab initio study of cyclic $(H_2O)_n$···HCl clusters by Packer and Clary.[5])

Details of the MC Simulation. A canonical Monte Carlo (MC) simulation was used, at $T = 50$ K. A fixed number of HCl molecules (18 or 79) was initially deposited at random on the cluster surface. First, $4 \times 10^7$ MC steps were carried out for HCl molecules only. Then $5 \times 10^8$ steps were performed on the entire system of HCl and $H_2O$ molecules. An MC step included a rotation and a translation of a randomly selected molecule. The translational steps were chosen from the Gaussian distribution, with $\sigma = 0.032$ and 0.08 Å for water and HCl, respectively. Rotation vectors $v_r$ were also selected from a Gaussian distribution as well, with $\sigma = 1.4°$ and 1.9° for water

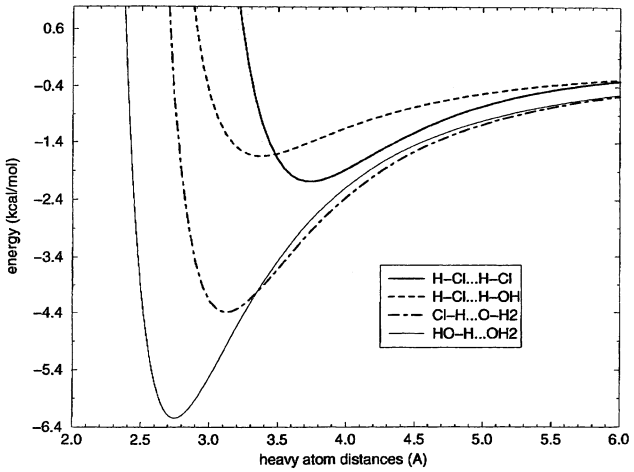


**Figure 2.** Intermolecular interactions. Thin solid line: TIP4P OH···O water−water interaction. Water orientations were set at minimum energy values. Dot−dashed: $H_2O$···HCl interaction. O···HCl is collinear with the water bisector. Dotted: HCl···HOH interaction. HCl···HO bonds are collinear. Thick solid: HCl···HCl, for a nonlinear minimum energy configuration.[72]

and HCl, respectively. Rotations were carried out around $v_r$ vectors according to formulas given in ref 75.

Definitions of Hydrogen Bonds. The discussion below employs a concept of intermolecular bonds. To define a "bond", radial distribution functions shown in Figure 3 were used, together with energy information obtained in a 79 HCl simulation. In the case of $H_2O$···$H_2O$ and $H_2O$···HCl, the geometric cutoff is conveniently set for a bond in the gap following the first near-neighbor peak in the radial distribution function, at 2.30 and 2.35 Å, respectively. The latter definition results in negative $H_2O$···HCl interactions with a mean value of −3.4 kcal/mol. Oxygen atoms of water with less than 2 hydrogen bonds *to other $H_2O$ molecules* are defined below as dangling (d-O), even if bonded to HCl. Dangling-H-atoms (d-H) of $H_2O$ correspond to zero hydrogen bonds to other $H_2O$.

In the case of HCl···HCl pairs, the separation of the near neighbor peak from the rest of the distribution is not as well defined. We tried two reasonable bond cutoffs, at 2.85 and 3.2 Å (see Figure 3c). Both definitions result in all-negative pair interactions, with mean values of −1.8 and −1.7 kcal/mol, respectively. The HCl···HOH bond cutoff was set at 2.89 Å. This is because $r < 2.89$ Å contributions to the radial distribution function shown in Figure 3b originate entirely from negative energy HCl interactions with d-H-atoms of the ice surface (mean interaction energy of −0.98 kcal/mol), whereas longer Cl···H distances correspond to both attractive and repulsive interactions with dangling and nondangling H. A shorter cutoff at 2.75 Å was tried as well, corresponding to a dip in the HCl···d-H distance distribution function.

*2.1.2. MC Results.* The results are shown in Figures 1, 3, and 4, and in Table 1. A distribution of HCl coordinations for the two coverages is shown in Table 1, for the short and long cutoff definitions. The two definitions yield qualitatively similar results.

Dangling-O-atoms of $H_2O$ provide strong binding sites for HCl. In the lowest coverage simulation, the number of d-O exceeds considerably the number of adsorbate molecules, and thus nearly all HCl are attached to d-O. One-third of adsorbate molecules form, in addition, a weak bond to a d-H in a two coordinated bridge configuration d-O···HCl···d-H (Table 1).

At the higher 79-molecule coverage, the number of adsorbate molecules exceeds the number of d-O binding sites. A moderate (∼16%) increase is observed in the total number of d-O sites, which occurs, presumably, at the expense of cleavage of strained $H_2O$···$H_2O$ bonds on the particle surface. (A similar but much more dramatic increase with coverage in the number of strong binding sites was observed in MC simulations of $NH_3$ adsorbate on the same ice particle.[61]) About 60% of HCl adsorbate molecules are bonded to surface O-atoms, a large majority of which are dangling. Nearly half of the O-bonded HCl molecules are doubly coordinated; i.e., an additional weak bond is formed by Cl, either to d-H of ice or to an H-atom of another HCl.

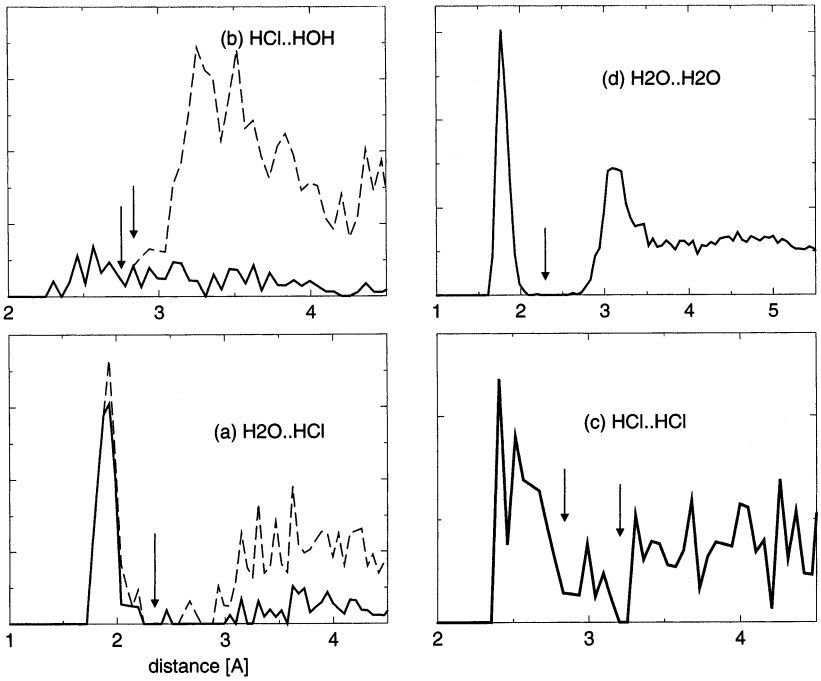


**Figure 3.** Radial distribution functions for H···X distances. Results from a 79 HCl simulation, unless explicitly stated otherwise. (a) (Dashed) H···O distances for $H_2O$···HCl pairs; (solid) dangling-O only. (b) (Dashed) Cl···H distances for $H_2O$···HCl pairs; (solid) d-H only. (c) Cl···H distances for HCl···HCl pairs. (d) O···H distances for $H_2O$···$H_2O$ pairs. The arrows denote cutoffs used for bond definitions.

**TABLE 1: HCl Coordinations**[a]

| | | |
|---|---|---|
| coverage[b] | 18 | 79 |
| total O-bonded | 17 | 46 |
| O···HCl[c] | 10 (9) | 17 (15) |
| O···HCl···d-H[d] | 6 (7) | 10 (13) |
| O···HCl···H(Cl)[e] | 1 (1) | 10 (14) |
| O···HCl···$H_2$ [f] | | 2 (4) |
| no O-bond[g] | 1 | 33 |
| Cl···HCl[h] | | 16 |
| Cl···HCl···H(Cl)[i] | | 8 |
| Cl···HCl···d-H[j] | 1 | 3 |
| no. of d-O | 43 | 50 |
| no. of d-H | 37 | 41 |
| no. of d-H···Cl(H) | 6 (8) | 17 (21) |

[a] Bond cutoffs: $H_2O$···$H_2O$, 2.30 Å; $H_2O$···HCl, 3.35 Å; HCl···HOH, 2.75 Å; HCl···HCl, 2.85 Å. Numbers in parentheses pertain to longer cutoffs: HCl···HOH, 2.89 Å; HCl···HCl, 3.20 Å; see text. Configurations of low abundance were omitted. [b] Number of HCl in the simulation. [c] A single bond to O-atoms, mostly d-O. [d] A two-coordinated bridge coordination. Most of the O-atoms and all H-atoms are dangling. [e] A two-coordinated bridge coordination, in which the Cl-atom is connected to H of another HCl. [f] Three-coordinated HCl. Cl is connected to H-atoms of two HCl. [g] HCl in which H-atom is not bonded to O of ice. At high coverage HCl engages in "worm like" configurations: HCl···HCl, HCl···HCl···HCl, etc. [h] "Worm tail" configuration. [i] "Worm middle" configuration. [j] "Worm tail" HCl, connected to d-H.

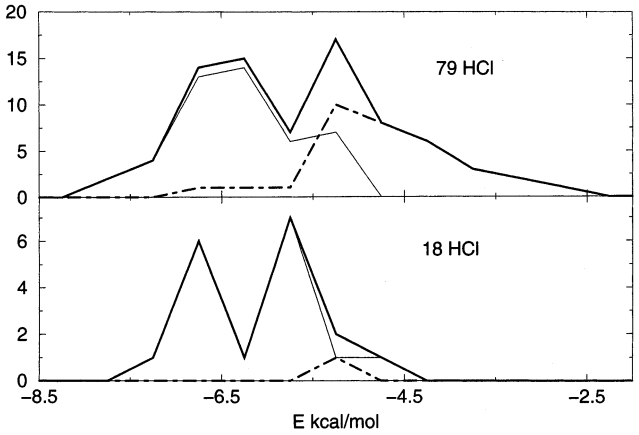


**Figure 4.** Distribution of molecular HCl energies, from the 50 K MC simulation at different coverages. The HCl energy was taken as a sum of its interactions with the particle and half of its interactions with other HCl. (Thick, solid) all HCl. (Thin, solid/dot−dashed) HCl with/without a hydrogen bond to an O-atom on the ice surface.

Triply coordinated HCl, with one bond to H and two to Cl are a minority species, even using the long bond cutoff. Most of the HCl that are not attached to the surface O-atoms participate in wormlike configurations such as HCl···HCl or HCl···HCl··· HCl. A head of a "worm" is commonly attached to a surface O-atom. A "worm-tail" may be terminated by a connection to d-H.

Figure 4 shows the distribution of the molecular binding energies. At the high coverage, the low and high energy wings of the distribution are dominated by HCl, which are and are not bonded to strong O-sites on the surface, respectively. For the low coverage, a doubly peaked structure is still observed, although nearly all molecules are O-bonded. The doubly coordinated HCl dominate the low energy peak in the molecular energy distribution. However, the division to two peaks does *not* correspond to the division between molecules with and without the extra weak bond to d-H. This finding underscores a significant contribution to the adsorbate binding energy from interactions with additional "non-bonded" water molecules.

*2.1.3. MC Conclusions and Comments.* In the present model, rigid un-ionizing adsorbate HCl is considered. The acid molecule is a good proton donor and a poor proton acceptor, and thus d-O-atoms of the ice surface serve as strong binding sites for the adsorbate. At low coverage, one-third of the HCl molecules form an additional weak bond to d-H. At higher coverage for which the number of HCl exceeds the number of d-O, two coordinated configurations of the form d-O···HCl···HCl are also present. Three coordinated configurations are uncommon.

Past studies suggest that the minimal number of bonds needed for HCl ionization is three: one to H, two to Cl.[7,9,11,44] However, an interesting situation appears to prevail on a cold particle surface: to ionize, molecular HCl needs three bonds, but as long as it is molecular, a third bond is not actively sought. The paucity of triply coordinated configurations is related to a relatively low density of surface d-H-atoms. As shown in the past,[69] the ice nanocrystal surface is characterized by a disordered structure, in which $H_2O$ molecules are mostly fully four-coordinated, albeit with a coordination shell strongly distorted from tetrahedral symmetry. Thus the cold ice-particle surface does not constitute a particularly effective solvating medium with respect to the acid.

However, the strength of HCl hydrogen bonds is expected to increase with hydrogen bond coordination (an effect that is absent in the present MC calculation). This is because hydrogen bonding stretches and polarizes HCl, which thus becomes a more effective hydrogen bonder. The implications will be discussed in the context of the interpretation of the spectra. Briefly, the MC calculation underestimates the ability of doubly coordinated HCl to reorganize the surrounding solvating medium.

**2.2. Ab Initio Calculations.** The MC simulations provide "entry level" molecular configurations adopted by adsorbate HCl on a cold particle surface. In this section, ab initio calculations on smaller clusters are used to elucidate the extent of HCl stretching and solvation in different configurations. Our MP2 level calculations include energy minimization and normal-mode analysis for $(H_2O)_n(HCl)_m$ clusters, with $m = 1, 2$, $n = 1-7$ (Figures 5 and 6). In larger clusters shown in Figure 6, the choice of HCl configurations was guided by the Monte Carlo results. The smaller structures (Figure 5) were added to elucidate trends with size.

*2.2.1. Computational Details.* The calculations were carried out with a suite of Gaussian 98 programs.[77] Full geometry optimizations were performed using the most stringent internal criteria ("verytight" option) at the MP2 frozen core level. Harmonic MP2 (frozen core) frequencies and infrared intensities were calculated using analytical second derivatives, except for the largest models $(H_2O)_7(HCl)$ (Figure 6j,l) for which the numerical option was used. The aug-cc-pVDZ basis set was employed in the calculations.[76] This basis set is the largest that could be realistically used with our computer resources for optimization and frequency calculations at a correlated level, for the largest cluster sizes. This basis set was retained for smaller clusters as well, to obtain trends as a function of size on a consistent level of accuracy. As shown previously, this basis set reproduces rather well geometries, frequencies, and electric properties of hydrogen-bonded clusters.[78] The HCl bond length, dipole moment, and fundamental harmonic frequency were calculated at the MP2 level as 1.288 Å, 1.185 D, and 3023 $cm^{-1}$, as compared to experimental values of 1.275 Å, 1.093 D, and 2991 $cm^{-1}$, respectively.[79] For $H_2O$, the OH bond length, HOH angle, dipole moment, and fundamental frequencies were calculated at the MP2 level as 0.966 Å, 103.9°, 1.879 D, and 3938, 3803, and 1622 $cm^{-1}$, as compared to experimental values

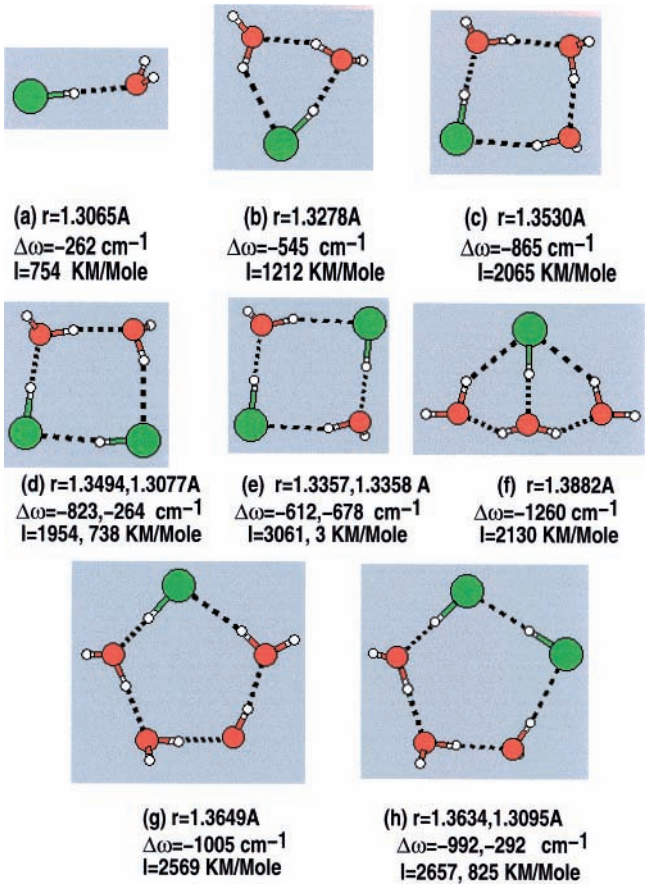


**Figure 5.** Cluster minima $(H_2O)_n(HCl)_m$, with $m = 1, 2$, $n = 1-4$, investigated in MP2/aug-cc-pvDZ calculations. HCl bond lengths, stretch frequency shifts, and intensities are marked.

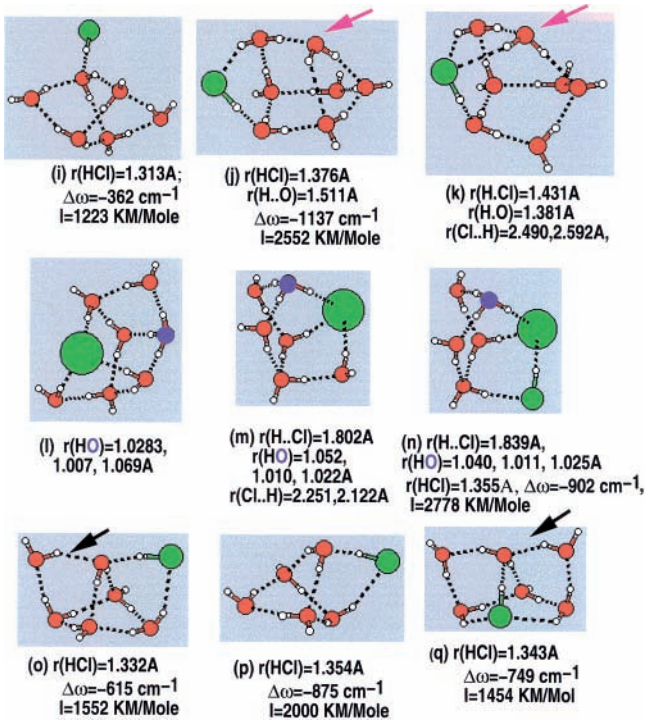


**Figure 6.** Cluster minima $(H_2O)_n(HCl)_m$, with $m = 1, 2$, $n = 5-7$, investigated in MP2/aug-cc-pvDZ calculations. HCl bond lengths, stretch frequency shifts, and intensities are marked for un-ionized acid molecules. In ionic clusters, the O-atom of $H_3O^+$ is blue. Purple arrows mark a water molecule in (j) that switched an H-bond to solvate chlorine in (k). Black arrows mark acceptor bonds that impede solvation by $H_2O$.

of 0.958 Å, 104.5°, 1.847 D, and 3942, 3832, and 1648 $cm^{-1}$, respectively.[80]

The MP2 method was judged to be more suitable to the current problem than the commonly employed and cheaper DFT/B3LYP, because the latter tends to overestimate the tendency of HCl to stretch and ionize. This conclusion was reached from a comparison of MP2 and DFT results in the aug-cc-pVDZ basis, and is in accord with past comparative studies employing MP2 and DFT with larger basis sets for $(H_2O)_n\cdots(HCl)$ clusters.[8,9] Table 2 shows HCl frequency shifts in $(H_2O)_n\cdots HCl$, $n = 1, 2$, with respect to isolated HCl, calculated with MP2 and DFT, and measured in the Ar matrix.[4] In the aug-cc-pVDZ basis, both methods overestimate the size of the shift; however, the agreement with experiment is much better for MP2. The present MP2 and DFT results are similar to MP2/6-31g-(2dp) and DFT/D95++(d,p) results of refs 5 and 7, respectively. One may note that structure f of $(H_2O)_3\cdots HCl$ in Figure 5 is molecular in MP2 but ionizes in B3LYP. (A similar result was reported for D95++(p,d) basis, but not for 6-311++g**.[8])

Inclusion of anharmonic effects was also attempted for structures for which HCl remains molecular. A local HCl stretch mode was assumed. The potential was mapped as a function of HCl bond length in the vicinity of the minimum and fitted to a Morse function. For isolated HCl, good agreement was obtained between the anharmonic Morse frequency, and the experiment (2916 versus 2886 $cm^{-1}$). Moreover, for the clusters, the harmonic Morse frequencies were within several tens of $cm^{-1}$ from the ones obtained from the normal-mode analysis. However, the anharmonic HCl frequency shifts in clusters are seriously overestimated. For example, the anharmonic shifts calculated for $H_2O\cdots HCl$ and $(H_2O)_2\cdots HCl$ were −327 and −743 $cm^{-1}$, respectively, as compared to the harmonic values of −262 and −545 $cm^{-1}$, and the experimental ones in an Ar matrix of −212 and 481 $cm^{-1}$.[4] Thus the deviation seems to increase with size. In the following discussion we empirically employ the harmonic values, because the latter are closer to the available experimental results.

**TABLE 2: HCl Frequency Shifts ($cm^{-1}$) in $(H_2O)_n\cdots(HCl)$ Clusters, $n = 1, 3$**

| n | exp[a] | MP2[b] | B3LYP[b] | B3LYP[c] | MP2[d] |
|---|---|---|---|---|---|
| 1 | −212 | −262 | −314 | −313 | −227 |
| 2 | −481 | −545 | −659 | −694 | −453 |
| 3 | | −865 | −1052 | −1199 | −727 |

[a] Reference 4. Experimental HCl frequencies obtained from mass-scaled values measured for deuterated clusters, in the Ar matrix. Frequency shifts with respect to HCl isolated in Ar. [b] Present results, aug-cc-pvDZ basis. [c] Reference 7. B3LYP/D95++(d,p). [d] Reference 5. MP2/6-31g(2dp). [e] In ref 4, a feature corresponding to −371 $cm^{-1}$ shift was tentatively assigned to $(H_2O)_3\cdots(HCl)$; but in view of computed trends this assignment appears unlikely.

Cluster energetics are reported in the Supporting Information. The CP correction[81] was applied to the optimum geometry for the full supermolecular basis. No account has been taken of BSSE in geometry optimization or in normal-mode analysis.

*2.2.2. Ab Initio Results.* The investigation included thirteen molecular structures (Figure 5a−h, Figure 6i,j,o−q), three ionized ones (Figure 6l−n), and one "semi-ionized" in Figure 6k. For the molecular structures, approximately linear correlation was found between HCl equilibrium bond length, and the frequency shift (Supporting Information, Figure A1). Molecular HCl transitions in the clusters are characterized by high intensity (700−3000 kM/mol). In accord with past studies,[5,7,9,11] all cyclic $(H_2O)_n\cdots(HCl)$ clusters shown in Figure 5 are molecular rather than ionic. The HCl frequency shift increases by 460 $cm^{-1}$ with

increasing ring size ($n = 2-4$) and concurrent reduction of the strain; a similar red shift as a function of ring size was observed in the hydrogen-bonded OH stretch band of cyclic pure water clusters.[82] The $(H_2O)_{1-3}\cdots(HCl)$ ring structures in Figure 5a−c correspond to the well-known lowest energy isomers.[5,7,9] The energy of the T-shaped structure (f) is 1290 $cm^{-1}$ higher than that of structure (c); (f) was included to demonstrate the remarkably high HCl frequency shift in this triply coordinated configuration. Each of the un-ionized structures calculated by us for the larger clusters is unlikely to be the *lowest* minimum for a given size. A number of past studies demonstrated both ionic and molecular minima of comparable energy already for $(H_2O)_4\cdots(HCl)$.[7−9] The objective here was to calculate HCl bond length and frequency *for a given pre-imposed coordination*, rather than to locate the lowest cluster minimum for a given size.

Three-dimensional structures shown in Figure 6 will be used for the interpretation of the experimental results for HCl adsorbate on ice. Cluster models with HCl coordination ranging from 1 to 3 were investigated, as suggested by MC simulations. A model with a singly coordinated HCl molecule was constructed by connecting HCl to a d-O-atom of the well-known water hexamer cage structure[83] (Figure 6i). The resulting HCl frequency shift with respect to the gas phase (−362 $cm^{-1}$) is in the range of the first experimentally observed band discussed in section 4. In model (j), HCl is in a doubly coordinated bridge configuration, with the H-atom connected to a d-O of the water cluster, and with Cl connected to a d-H. The resulting HCl bond stretching is substantial, but proton transfer does not occur as yet; the H-atom is closer to Cl (1.376 Å) than to O (1.511 Å). The large calculated frequency shift (−1137 $cm^{-1}$) is close to the shift observed for the second molecular band (−1186 $cm^{-1}$). A model with triply coordinated HCl was constructed by replacing, with HCl, one of the water molecules in a low energy water heptamer structure.[84] The triply coordinated HCl dissociated in the course of minimization, forming a clearly recognizable solvated $H_3O^+$ and $Cl^-$ contact-ion pair (Figure 6m).

A question can be asked concerning the ability of HCl to solvate another HCl on the Cl side, in place of $H_2O$. This is because, according to Monte Carlo modeling at the higher coverages, the Cl side of HCl is frequently solvated by another HCl. To address this issue, two water molecules of the heptamer were each replaced by an HCl. The ensuing minimization resulted in an ionized minimum (Figure 6n), which is very similar to structure (m), with $Cl^-$ solvated by the second HCl instead of $H_2O$. Moreover, in cyclic molecular minima $(HCl)(H_2O)_{n=3,4}$, replacement of an $H_2O$ molecule by a second HCl in tandem to the first was calculated to have only a minor effect (of a few tens of $cm^{-1}$) on the first HCl frequency; compare structures (c) and (d) and (g) and (h) in Figure 5. *Thus it appears that the Cl side of HCl can be solvated almost as effectively by another HCl, as by $H_2O$, both in molecular and in ionized structures.* Moreover, calculations show that HCl molecules, solvating Cl ends of strongly stretched molecular HCl (as in Figure 5d,h), are characterized by a few hundred $cm^{-1}$ red shift and thus contribute to the first observed spectral band.[85] A much larger shift was obtained for HCl solvating $Cl^-$. An intense transition was calculated at 2121 $cm^{-1}$ for HCl solvating $Cl^-$ in the ionized structure (n); this result is used below in the assignment of one of the experimentally observed bands.

High coordination of HCl is necessary but insufficient for effective acid solvation. For example, structures (o) and (q) in Figure 6 include doubly and triply coordinated HCl molecules, which, however, are only moderately stretched in contrast to structures (j) and (m). Thus, an additional requirement pertains to the coordination of proton−acceptor $H_2O$ that is bonded to the H-atom of HCl. As discussed in past theoretical studies of proton transfer in water, [51,52] $H_2O$ is an effective proton acceptor only if both H-atoms are hydrogen bonded to other $H_2O$, and the O does not have an additional acceptor bond from another $H_2O$. An arrow marks the "offending" proton acceptor bond in structures (o) and (q), which impedes solvation. To further probe this effect, the "offending" bond in structure (o) was removed by elimination of the $H_2O$ molecule in the top left corner with the resulting structure subjected to energy minimization. A substantial increase in the HCl bond length was in fact obtained in the minimized structure (p), as compared to (o), from 1.332 to 1.354 Å, with concurrent increase in the *frequency shift*, from −615 to −875 $cm^{-1}$.

One may note finally the T-shaped structure $(H_2O)_3\cdots HCl$ in Figure 5f in which HCl is molecular (albeit strongly stretched), despite triple coordination. Apparently, the two edge water molecules are insufficient to solvate simultaneously $H_3O^+$ and $Cl^-$.

Another striking ab initio result is the common presence of flat potential energy regions connecting different bonding structures. Because of that presence, lengthy minimizations were needed; e.g., minimization of the cyclic structure (h) was interrupted after 128 iterations, still yielding one imaginary frequency. The remaining structures in Figures 5 and 6 yielded only real frequencies. However, upon extended minimization of the singly coordinated structure (i), the Gaussian program located an essentially barrierless transition to the lower energy doubly coordinated structure (o). Similarly, extended minimization of the doubly coordinated structure (j) resulted in an essentially barrierless transition to the "semi-ionized" structure (k). The latter transition corresponds to cleavage of a strained hydrogen bond in a three-membered water ring, and reattachment of the corresponding water H-atom to Cl. Thus the acid molecule becomes triply coordinated, although the two solvating hydrogen bonds to Cl are relatively long. (Compare bond lengths in (k) and (m).) The result is *partial* proton transfer from acid to water; the proton adopts a location roughly in the middle between O and Cl, rather than forming an $H_3O^+$ unit as in (m) and (n). The energy difference between pairs of structures (i) and (o), and (j) and (k), is only a few hundred $cm^{-1}$, well below the zero-point energy. Similar transitions are likely to occur, with zero or small activation barriers, on the ice surface (and are discussed in section 4).

An ion-separated structure (l) was obtained from molecular structure (j) by subjecting it to DFT minimization. (As noted above, DFT overestimates the tendency of HCl to stretch and ionize.) Structure (l) is a minimum in MP2 as well; its energy is 2054 $cm^{-1}$ below that of (j). This result is in qualitative accord with activated but irreversible ionization observed in the experiment for HCl adsorbate (section 4). Although the MP2 reaction path was not calculated, comparison between (j) and (l) is instructive because it may represent the type of changes occurring during adsorbate ionization. A striking feature is collective participation of numerous molecules in the transition. Two proton jumps occur, resulting in an $H_3O^+$ ion at a next-near-neighbor position with respect to $Cl^-$. Out of eleven hydrogen bonds in (j), three are broken, and two new ones are formed. One bond undergoes a donor−acceptor switch. The cooperative nature of the ionization transition was already noted in several past electronic-structure studies of acid ionization in clusters.[6,8,10]

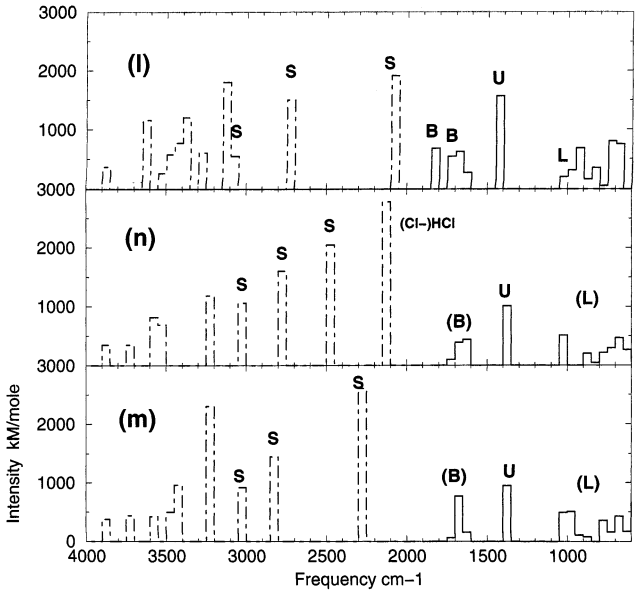


**Figure 7.** Ab initio spectra of ionic structures (l−n) (see Figure 5). Intensities below 1900 $cm^{-1}$ (solid lines) were multiplied by 4. (Dot−dashed) stretch mode. S, B, U, and L denote stretch, bending, umbrella, and libration modes of $H_3O^+$; brackets denote mixed modes with $H_2O$. Note the 2121 $cm^{-1}$ frequency of HCl bonded to $Cl^-$ in the middle panel.

Finally, the normal mode spectra of the three ionic structures (l−n) are shown in Figure 7; the spectra will be used in the interpretation of ionized adsorbate and hydrate spectra. For $H_3O^+$, the lowest frequency and the most intense OH-stretch peak originates from the most elongated OH. In models (m) and (n) with contact ion pairing, the longest OH is in contact with the anion; the corresponding frequencies are 2292 and 2497 $cm^{-1}$, respectively. In model (l), $H_3O^+$ is distorted toward the Zundel structure, with one OH significantly longer than the other two. The corresponding normal frequency is 2059 $cm^{-1}$; in anharmonic reality, such long bonds most likely contribute to the Zundel continuum. The frequencies of the two remaining $H_3O^+$-stretch transitions are similar for all three structures, falling in ranges 2710−2803 and 3032−3077 $cm^{-1}$.

*2.2.3. Ab Initio Conclusions and Comments.* Efforts were made to construct reasonable cluster models, which are sufficiently large to represent unstrained hydrogen bonding of molecular and ionized HCl adsorbate to the ice particle surfaces, and yet sufficiently small to be amenable to ab initio studies. The highest level of calculation feasible for us was MP2/aug-cc-pVDZ.

The extent of HCl stretching and the corresponding frequency shift are influenced by several factors: the HCl coordination, the extent of strain in the hydrogen bond network, and the coordination of the proton acceptor water molecule. Singly and doubly coordinated HCl remains molecular. Ab initio frequency shifts calculated for singly and doubly coordinated HCl in models (i) and (j) (Figure 6) (−362 and −1137 $cm^{-1}$) are close to the first and second measured bands (section 4). The larger shift appears to require, in addition to double coordination d-O···HCl···d-H, a relatively unstrained hydrogen bond network, because a smaller model (p) of similar coordination resulted in a significantly reduced shift. Barrierless ionization was obtained in triply coordinated models, with one bond to H and two bonds to Cl; this result is in accord with past ab initio studies.[7,9,11,44] One may note also the triply coordinated but strained configuration (k), in which proton-sharing occurs between water and chloride. Solvation of the Cl side of HCl by another HCl appears to be as effective as by H-atoms of water. In addition, solvation is most effective if both H-atoms of the proton acceptor $H_2O$ are bonded to other water molecules, whereas the O-atom is *not* engaged in a proton acceptor bond with another water. The latter acceptor bond, if present, impedes stretching of doubly coordinated HCl and prevents proton transfer from a triply coordinated one (see structures (o) and (q)).

Calculations suggest a common presence of barrierless or low barrier transitions between distinct bonding structures (e.g., structures (i) and (n); (j), (k), and (l)). This conclusion should be regarded as tentative, because potential surfaces calculated on the present ab initio level appear to be too flat (as evidenced by the overestimation of the anharmonic frequency shifts). Moreover, the hydrogen bond network of the much larger ice nanoparticles may be more rigid. Still, this finding appears consistent with the experimental evidence for low barrier transitions between molecular and ionic adsorbate states. Probable presence of numerous bonding structures below the zero-point energy complicates interpretation of the spectra, as discussed in sections 4 and 5.

## 3. Experimental Section

The usual difficulty in the investigation of adsorbate−surface spectroscopy is a large interior-to-surface ratio of molecules, so that spectroscopic signals are lost among those of the bulk substance. In the present study, this problem is overcome by the use of 3-D arrays of ice nanocrystals that assemble on the windows of a collisional-cooling cluster cell. The arrays prepared at 50 K are stable at temperatures below 100 K and offer a large surface area with respect to gas adsorption; their surface properties are similar to those of an ice aerosol.[67] The mean diameter of the constituent nanoparticles is reflected in the intensity ratio of the d-H spectral feature, originating from the surface, and the hydrogen bonded OH band, caused predominantly by interior water molecules. This size estimate has been double-checked by measurement of the intensity of a $CF_4$ adsorbate band for monolayer coverage. (Monolayer coverage is detected from the unique band shape characteristic of collective LO and TO modes of adsorbate $CF_4$.[66])

The above system has been used to investigate transmission FTIR spectra of bare and adsorbate covered ice nanoparticles in the 50−120 K range. Samples have been prepared of HCl adsorbed on $H_2O$, DCl on $D_2O$, HCl on $D_2O$, DCl on $H_2O$, and HBr on $H_2O$ ice. The measurements focused on the difference spectra between adsorbate-covered nanocrystals and bare nanocrystals prepared under similar conditions. The differencing allows for a clear view of spectral features originating from the adsorbate.

An earlier FTIR study of HCl adsorbed on ice nanocrystal arrays showed that, to reveal the details of the surface adsorbed state, control of the formation of the adsorbate layer is critical. In that study,[24] HCl was adsorbed by vapor diffusion to ice nanocrystals within 3-D arrays supported on the two infrared-transparent windows of a static cluster cell. This resulted in nonuniform coverage of the particle surfaces as the HCl uptake varied greatly from the front to the backside of the arrays. The computations of section 2 show that solvation by other HCl molecules is nearly as effective as hydration in stabilizing the ionized state. The high surface concentration of HCl at the front of the arrays caused extensive ionization, so that intense ionic bands dominated much of each spectrum (see Figure 3B of ref 24). Observation of the bands of molecularly adsorbed HCl was therefore severely restricted.

Here, in a broad-ranging search for the stretch-mode bands of molecular HCl, DCl, and HBr adsorbed at submonolayer

levels on the surface of crystalline ice nanoparticles, we have adopted an approach that avoids this large variation in acid coverage throughout an array. In this approach, nanocrystals of cubic ice,[86] ~12 nm in average diameter, were formed as aerosol particles by rapid loading of the double-walled cluster cell to 0.4 bar with 1% mixtures of water vapor in helium. With the thick-walled inner chamber held at 50 K, ~6% of the ice particles instantaneously collect on the ZnS cell windows.[67] A dozen repetitive cycles of loading and pumping produces 3-D arrays having an effective thickness of ~0.4 $\mu$m.

Hydrogen chloride was included in the ice arrays, with an overall acid-to-water ratio of ~1:50, by alternating each loading of ice particles with a loading of much smaller clusters of HCl or DCl. At 50 K, the acid clusters are a transient part of the 3-D array. Much of the HCl moves immediately to the surface of the ice particles with the remainder following when the cell is warmed to 60 K. Though this approach does not give completely uniform distributions of acid molecules on the particle surfaces, superiority to previous methods is evident from the relatively weak intensity of interfering ionic bands. For 12 nm ice particles, ~12% of the water molecules are part of the surface,[69] and thus the standard acid dosage was ~1 adsorbed HCl for each six surface water molecules. Ice arrays dosed with HBr have been similarly prepared. The experimental adsorbate coverage was estimated from the observed decrease in the free d-H (D) band intensity at 3694 (2726) $cm^{-1}$.[67]

Because Ostwald ripening of 12 nm ice nanocrystals occurs above 100 K and is aggressive at 120 K, most of the present results refer to the temperature range 50−110 K. (Ostwald ripening refers to the growth of larger particles at the expense of the smaller ones driven by the greater vapor pressure of the latter.)

## 4. Results and Discussion: Acid−Adsorbate Spectra on Surfaces of Ice Nanocrystals

**4.1. Overview of 60 K Adsorbate Spectra.** The measured difference spectra are shown in Figures 8−12. At 50−60 K, the spectra display two broad bands, which are assigned to molecular HCl, DCl, and HBr (Figures 8-11). As the temperature is raised, ionic features grow (Figures 9−11). Different responses to warming are observed depending on the level of acid doping of the ice surface. Dosage levels of ~20% of a monolayer typically result in limited ionization during preparation followed by progressive low levels of ion-pair formation in the 70−90 K range. Such samples then display a burst of ionization in the 90−95 K range with the difference spectra becoming dominated by bands characteristic of the acid hydrates. The highest dosage levels (≥30%) are accompanied by significant ionization already during sample preparation at 50 K, followed by extensive ionization above 60 K. Still, near 90 K, a large jump is observed in the ion signal. Low acid dose levels <20% are associated with a gradual increase in the ion bands, but without a burst of ionization. Rather, progressive ionization continues to higher temperatures, with the molecular band (1) still visible at temperatures as high as 110 K.

The Zundel effect, i.e., a very intense continuum absorption underlying the distinct bands, is prominent in the measured spectra. The continuum contribution (which is suppressed in Figures 8−11 for a clearer view of the bands) can be seen in Figure 12.

*4.1.1. Molecular Bands of Adsorbate HCl and HBr at 50−60 K.* Examples of difference spectra, of ice arrays with adsorbed HCl compared with bare-ice arrays, are given in Figure 8. The spectra, obtained at 50 K using surface coatings of ~20%, are

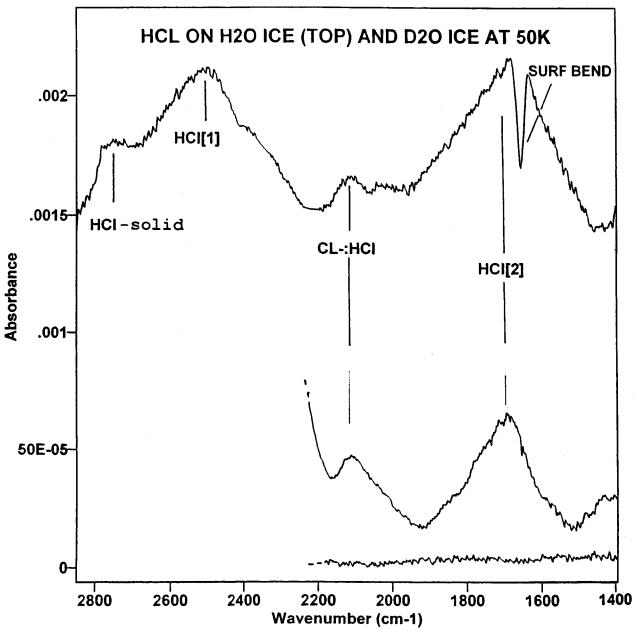


**Figure 8.** Infrared difference spectra at 50 K from comparison of nanocrystalline arrays with ~20% cover of HCl with similar bare-particle arrays. The top and middle spectra are for $H_2O$ and $D_2O$ ice-particle arrays, respectively. Large fluctuations in the O−D stretch region of the latter have been blanked out. The bottom difference spectrum, comparing two pure $D_2O$ ice samples, illustrates the instrumental noise.

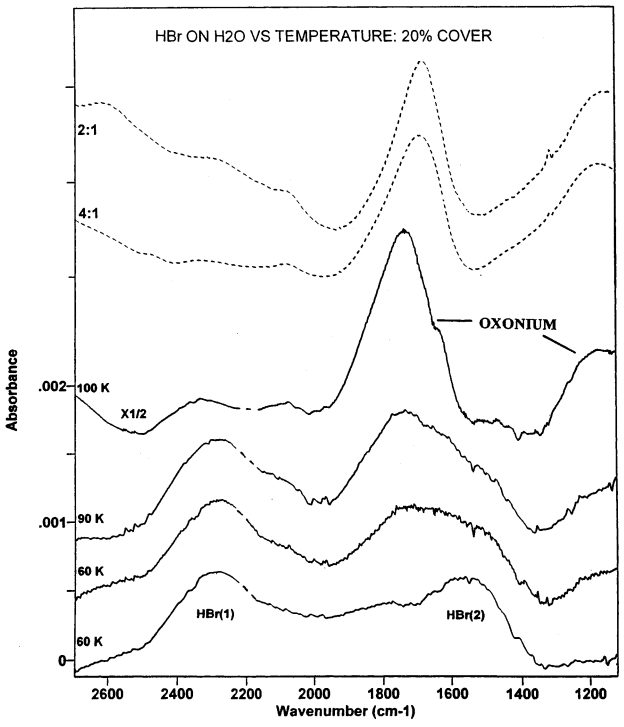


**Figure 9.** Infrared difference spectra for HBr on $H_2O$ for ice arrays with moderate acid dosing (~20% of a monolayer cover). Spectra are offset to show the temperature dependence of the acid−ice interaction. The spectra labeled 2:1 and 4:1 are of the corresponding $H_2O$:HBr amorphous hydrate nanoparticles. Note: weak ion bands at 2070 and 1670 $cm^{-1}$ have been subtracted from the bottom spectrum, the 100 K spectrum has been compressed 2-fold, and the Zundel continuum has been suppressed.

for HCl adsorbed on $H_2O$ ice (top) and for HCl on $D_2O$ ice (middle). The HCl(1) band, observed in previous studies, is apparent at 2480 $cm^{-1}$ in the top spectrum, together with a second band of molecular HCl indicated near 1700 $cm^{-1}$.

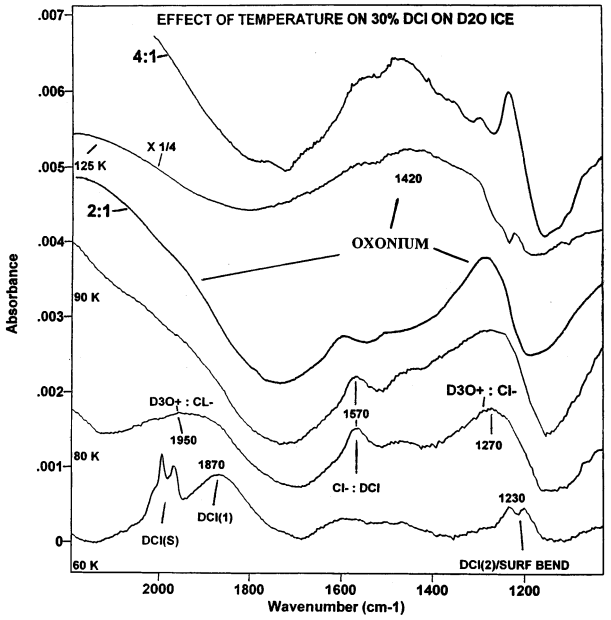


**Figure 10.** As in Figure 9, except for DCl on $D_2O$ ice with a higher acid dosage (~30% of a monolayer), and a 4-fold compression of the 125 K spectrum. The spectra labeled 2:1 and 4:1 are of the corresponding amorphous films (Figure 1).

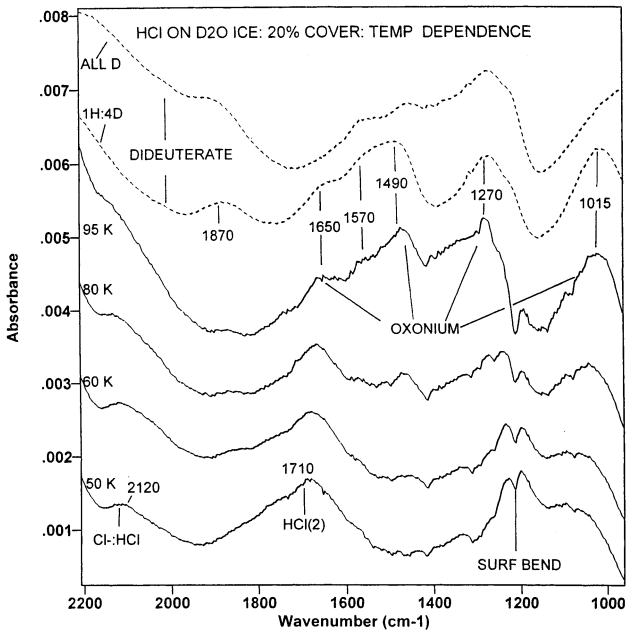


**Figure 11.** As in Figure 9, except for HCl adsorbate on $D_2O$ ice (20% monolayer). For comparison, the two top dashed spectra are of 70 K amorphous dideuterate aerosols with two isotopic compositions (all D, and 1H:4D with complete isotopic scrambling).

However, the oxonium ion has a known band of moderate intensity near 1700 $cm^{-1}$.[15] The experiment was carried out under conditions corresponding to minimal ionization (low coverage, low temperature). Still, because of the overlapping ion band, together with interference from the surface water-bending band near 1650 $cm^{-1}$, the 1700 $cm^{-1}$ band cannot be assigned with confidence to molecular HCl, on the basis of the top spectrum alone. (The surface water-bending frequency is affected by the adsorbate, resulting in a dip in the HCl(2) band.)

Fortunately, both interferences in the top spectrum of Figure 8 can be shifted out of the 1700 $cm^{-1}$ region by adsorbing HCl on nanocrystals of $D_2O$ rather than $H_2O$. The 1H:4D dihydrate spectrum of Figure 11 shows that isotopically mixed oxonium

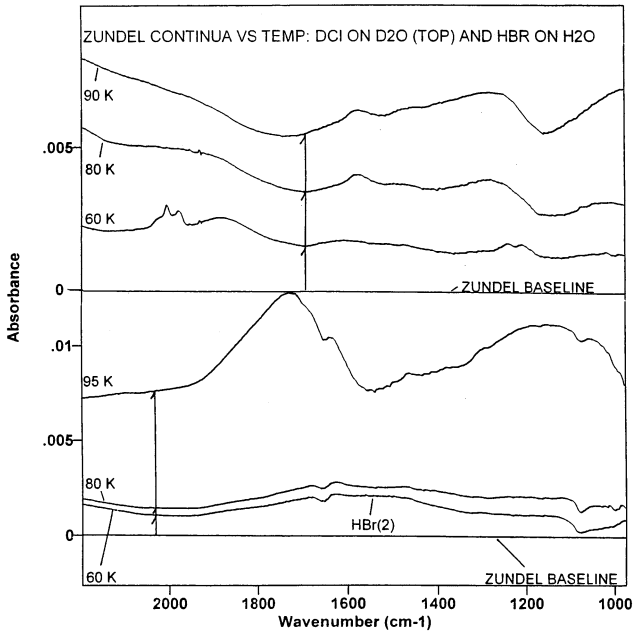


**Figure 12.** Difference infrared spectra of HBr on $H_2O$ (bottom) and DCl on $D_2O$ ice nanocrystals as a function of temperature showing the Zundel continua that are suppressed in Figures 9 and 11. Here each spectrum is referenced to a baseline extended from frequencies above the Zundel continuum. The vertical arrows at corresponding frequencies of the H and D systems indicate approximate magnitudes of the continua.

ions (such as $HD_2O^+$ and $HD_4O_2^+$, the low temperature ionization products for HCl on $D_2O$) have no structured absorption in the 1700 $cm^{-1}$ region. The band of the surface water-bending mode is meanwhile moved to ~1200 $cm^{-1}$. Despite this elimination of the interfering features, a band at ~1700 $cm^{-1}$ remains in the surface spectrum (Figure 8 (middle)). The computational results have identified likely structures (Figure 6i,j), formed by HCl with ice-surface groups, capable of inducing small (~400 $cm^{-1}$) and large (>1000 $cm^{-1}$) shifts of the HCl stretch mode relative to the HCl gas-phase frequency. Together with the two spectra of Figure 8, these results identify molecularly adsorbed HCl as the source of prominent bands near 2480 and 1700 $cm^{-1}$ (corresponding to frequency shifts of −406 and −1186 $cm^{-1}$ with respect to the gas phase).

Further experimental evidence, that the stretch mode of molecular HCl strongly bound to the ice surface absorbs near 1700 $cm^{-1}$, has been obtained from the analogous difference spectra of HBr adsorbed on $H_2O$ (Figure 9) and $D_2O$ ice arrays. Because a combination of the weaker bond and greater mass of HBr causes a lower gas-phase stretch-mode frequency (2560 vs 2891 $cm^{-1}$),[87] red-shifted analogues of the two bands of molecularly adsorbed HCl are expected. That two such bands are present in the 60 K difference spectra of HBr on $H_2O$ is apparent from the bottom spectrum of Figure 9. The weakly shifted HBr(1) mode appears as a broad band near 2260 $cm^{-1}$. A second prominent band near 1530 $cm^{-1}$ is logically attributed to the strongly bound HBr(2). A band of similar position and bandwidth is also present in the spectrum of HBr adsorbed on $D_2O$ ice (not shown).

The two bands in the spectra of molecularly adsorbed HCl and HBr do not include all of the infrared absorption by molecularly adsorbed acid molecules. As indicated in Figures 8 and 9, and consistent with computational results (section 2), subbands and diffuse absorption are present between the band maxima for both HCl and HBr. In particular, the MP2

calculations identify the weak band at 2120 $cm^{-1}$ in Figure 8 with acid molecules that solvate $Cl^-$, as in Figure 6n. The corresponding band for HBr appears near 2070 $cm^{-1}$.

*4.1.2. The 50−60 K Adsorbate Spectra: Discussion.* The HCl(1) band in Figure 8, with a frequency downshifted by ∼400 $cm^{-1}$ with respect to the HCl gas phase, indicates slightly stretched HCl, whereas the HCl(2) band, corresponding to a huge frequency downshift of ∼1200 $cm^{-1}$, points to strongly stretched HCl on the verge of ionization.

According to the MC simulations of the molecular adsorbate state at 50 K, the typical coordination of HCl is either one or two. That is, HCl bonds preferentially to dangling-O-atoms on the ice surface, with about one-third of the acid molecules acquiring an additional bond, via Cl, to a d-H-atom in the vicinity. The experimental coverage of 20% was determined from the observed decrease in the free d-H intensity. The ∼1:3 ratio of doubly and singly coordinated molecules, as obtained by MC, suggests that the percentage of bonded d-O-atoms on the nanoparticle surface is much higher than that of d-H, i.e., closer to 80%.

Ab initio cluster calculations confirm that singly and doubly coordinated HCl remains molecular. The ab initio frequency shift calculated for singly coordinated HCl bonded to a d-O in a water cluster (Figure 6i) is close to the first measured band. A cluster model shown in Figure 6j, in which HCl is in a doubly coordinated bridge configuration d-O···HCl···d-H, yielded a large frequency shift similar to that of the second measured band. Comparable intensities measured for the two molecular bands (Figure 8a) appear consistent with the ∼1:3 abundance ratio of singly and doubly coordinated HCl. This is because the ab initio intensity of the HCl stretch in configuration (j) is 2 times that of (i). According to the MC simulations, triply coordinated configurations that lead to ionization are improbable because of scarcity of d-H-atoms on the ice particle surface.

However, the large frequency shift of the doubly coordinated HCl is contingent on a relatively unstrained hydrogen-bond network. Moreover, the large shift of the doubly coordinated HCl is obtained only if the acceptor d-O molecule *does not have an additional acceptor bond from another $H_2O$* (see section 2.1). The observation of strongly stretched HCl indicates that doubly coordinated acid molecules are able to modify their solvation shells beyond the MC results. This is because all d-O molecules in the MC simulations have interfering acceptor bonds from other water molecules. In reality, the presence of the 1700 $cm^{-1}$ band already at 50 K indicates efficient elimination of such acceptor bonds in a low activation-energy process. The elimination process is likely to be promoted by the strengthening of the remaining hydrogen bonds, due to HCl polarization that accompanies the stretching. (HCl polarization and stretching were not included in MC.) Observation of the 2120 $cm^{-1}$ band of $Cl^-$···HCl indicates that some polarized HCl molecules manage to acquire a third bond to another HCl and to ionize. (Ab initio calculations show that the chloride can be solvated by HCl, much as by $H_2O$.)

The presence of an additional molecular configuration, d-O··· HCl···HCl, was suggested by the MC simulations for coverages that saturate the d-O sites. An unstrained cyclic ab initio model of Figure 5h suggests that the first and the second HCl in such configurations contribute to HCl(2) and HCl(1) bands, respectively.[85] (Note that there is some inhomogeneity in the experimental surface coverage, with acid self-solvation most important in the more dense spots.)

**4.2. Temperature Effect on Adsorbate Bands; Transition from Molecular Adsorbate to Ionized Surface Hydrate Phase.** The evolution of the DCl/$D_2O$ spectra as a function of temperature can be noted in Figure 10. Spectra of 30% DCl on $D_2O$ nanocrystals obtained at 60 K are dominated by a band of molecularly adsorbed acid (DCl(1)) at 1870 $cm^{-1}$ (Figure 10, bottom). The position of this band is consistent with previous reports[15,24] and with the frequency of the corresponding HCl-(1) band (2480 $cm^{-1}$). On the basis of the computational and experimental results for HCl, a band of molecular DCl(2) is expected in the 1200−1300 $cm^{-1}$ range. A band is in fact visible near 1230 $cm^{-1}$; however, as in the case of HCl/$H_2O$, assignment is problematic due to interfering features from both an oxonium-ion band near 1270 $cm^{-1}$ and the bending mode[69b] of the ice-surface molecules at 1213 $cm^{-1}$ (the latter appears also in the 125 K adsorbate spectrum). To avoid this interference, scans have been made for DCl on the $H_2O$ ice surface (not shown) which confirm the assignment as a DCl(2) band centered at ∼1230 $cm^{-1}$.

The analysis of the system evolution upon heating is based on the assignment of the acid-deuterate bands (see Appendix I). Heating to 80 K is associated with gradual growth of ionic features at 1950, 1570, and 1270 $cm^{-1}$. Presumably, some of the doubly coordinated DCl molecules acquire a third hydrogen bond and undergo ionization, forming contact ion pairs. Acquisition of a third bond is a low activation energy process, likely to be associated with DCl surface diffusion, or cleaving of the most strained hydrogen bonds within the ice surface. In accord with discussion in Appendix I, the band at 1950 $cm^{-1}$ is assigned to the OD stretch of a $D_3O^+$ cation in contact with $Cl^-$. The feature at 1270 $cm^{-1}$ is contributed by ion bending (probably with admixture of water bending). The feature at 1570 $cm^{-1}$ originates from the stretch vibration of DCl solvating $Cl^-$ ions, supporting the notion that self-solvation by acid molecules plays an important role in initial stages of ionization.

A structural transition of the adsorbate−surface system to an ionic hydrate phase is initiated at 90 K. The 1950 $cm^{-1}$ feature of contact ion pairs is no longer prominent, and the $Cl^-$···DCl feature at 1570 $cm^{-1}$ is reduced. At this stage, the spectrum resembles that of the amorphous acid dideuterate, including the underlying continuum indicative of the Zundel-ion formation. (The Zundel effect is discussed in more detail below.) Further heating to 125 K results in more extensive hydration and ion separation, as evidenced by the resemblance of the spectrum to that of amorphous tetradeuterate. However, at this temperature acid hydration is likely to be influenced by water-vapor deposition due to Ostwald ripening (i.e., evaporation of the smallest ice nanoparticles, which is significant above 110 K).

A closely related evolution with increasing temperature is observed for 20% HBr on $H_2O$ (Figure 9). Due to low coverage, there is minimal (but observable) evidence of ionization below 90 K. That is, between 60 and 90 K the ∼1700 $cm^{-1}$ oxonium-ion band intensifies; but the molecular bands remain prominent until the ionization burst at ∼95 K. In fact, at 90 K, the HBr(1) band is essentially unchanged whereas the HBr(2) band has weakened noticeably, suggesting that primarily the highly stretched acid molecules described by the calculations of section 2 are on the verge of ionization at the lower temperatures. Note the dramatic change from a "largely molecular" spectrum at 90 K, to the much more intense ionic hydrate-like spectrum at 100 K. The 100 K surface spectrum appears closer to that of the tetrahydrate than dihydrate. (Reduced intensity near 2500 $cm^{-1}$ in the surface and tetrahydrate spectra, as compared to the dihydrate spectrum, is indicative of a reduced amount of contact ion pairing; see Appendix I.)

The temperature dependence of the HCl-on-$D_2O$-ice spectrum, at 20% coverage, can be followed in Figure 11. The 50 K spectrum at the bottom includes the molecular HCl(2) feature of strongly stretched HCl, and a 2120 $cm^{-1}$ feature of HCl solvating the anion (as before, some ionization is present already at 50 K). A growth of ionic features is associated with heating; however, the molecular HCl(2) band is still apparent at 80 K. At 95 K the transition to an ionic surface phase has occurred. The 95 K surface spectrum is similar to that of an isotopically scrambled ionic dideuterate film, prepared from a $1HCl:2D_2O$ mixture (1H:4D ratio; bottom of the two dashed curves), but not that of an all-D dideuterate (top, Figure 11). This result demonstrates that the 95 K ionic phase is a *surface* phase formed from the acid adsorbate and the surface water molecules in the $1HCl:2D_2O$ ratio; otherwise, a spectroscopic signature of a much more completely deuterated system would be obtained.

The d-H (D) feature, appearing at 3694 (2726) $cm^{-1}$, for free-OH (OD) unbonded to adsorbate is a useful spectroscopic probe of the ice/adsorbate system.[67] At acid coverages of ~40%, the transition to a tetrahydrate-like phase is associated with nearly complete disappearance of this feature. At the ionization burst of the 20% cases, the loss roughly doubles over that at 50 K to a total loss of 30−40%.

**4.3. Continuum Absorption: The Surface Zundel Effect.** The surface Zundel effect is highlighted in Figure 12. Specifically, $HBr/H_2O$ and $DCl/D_2O$ spectra, like those shown in Figures 9 and 10, are redisplayed with the underlying continua included. The baseline was established and extended from above 3000 $cm^{-1}$ for $DCl/D_2O$, and 3600 $cm^{-1}$ for $HBr/H_2O$. In the case of $HBr/H_2O$, an abrupt large increase of continuum intensity is observed at 95 K, which coincides with the transition from predominantly molecular to ionic surface bands. In the $DCl/D_2O$ sample, a more gradual increase is observed in the continuum signal; the concurrent increase between 60 and 80 K of the hydronium contact-ion-pair signature was noted above.

In the high temperature limit, the Zundel effect is consistent with the good match of the spectral bands to those of amorphous hydrates/deuterates (Figures 9 and 10, top portion). A similar continuum can be seen underlying the bands of the dideuterate film in Figure 13. The relative contribution of the continuum, as compared to the discrete band intensities, seems enhanced by a factor of 1.5−2 in the surface spectra, relative to the film. The surface dideuterate layer most likely includes Zundel ions as the dominant cation species, because the structure of the crystal dihydrate analogue was shown to be $(H_5O_2^+)(Cl^-)$.[58] Still, the OD stretch spectrum of the amorphous solid suggests a continuous distribution of structures ranging from Zundel to hydronium (see Appendix I).

A number of interesting questions can be asked about the higher-*T* surface spectra but are beyond our current theoretical tools. What is the relative contribution of the static and dynamic fluctuations; i.e., is the Zundel continuum dominated by a continuous distribution of "equilibrium" ionic structures, or by dynamic modulation of the proton in the Zundel-like members of the distribution? One may note current efforts to address such questions theoretically for liquid acid solutions, with the help of extended valence bond models.[54,55,88]

Another uncertainty pertains to the source of the large Zundel intensity. The integrated continuum intensity per deuteron in the amorphous dideuterate is about 2 times larger than that of the already strong OD stretch band, per D-atom. As noted above, there is a further enhancement by a factor of 1.5−2 for the ionized adsorbate layer. This remarkable continuum intensity suggests the occurrence of large-amplitude fluctuations of the charge distribution, induced by the radiation and magnified by the freedom of motion in the surface layer. The high continuum intensity in protonated systems was discussed in the past in terms of high polarizability of the Zundel proton in the fluctuating potential well.[57] Additional effects may be present in the surface layer; e.g., excitations contributing to the continuum may be associated with proton motion involving a transition over a whole range of bonding configurations. In fact, current diffusion Monte Carlo simulations of protonated water clusters $H^+(H_2O)_{n=6-8}$ reveal numerous bonding configurations (i.e., minima) already within the range of the zero-point motion.[89]

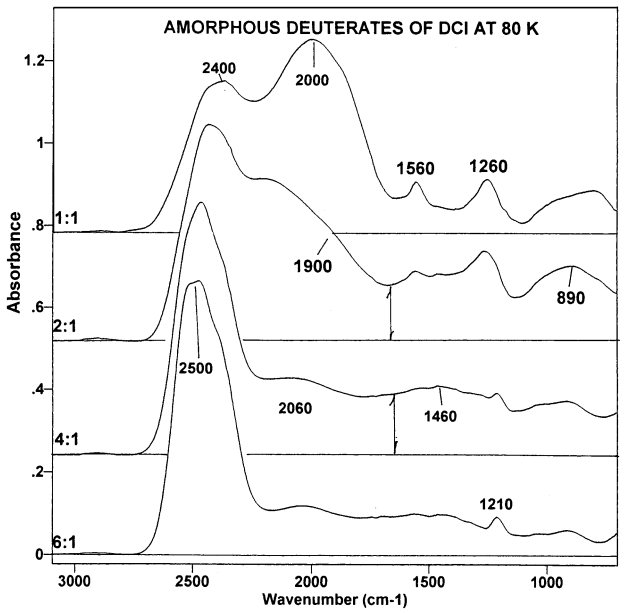


**Figure 13.** Infrared absorbance of amorphous deuterate films of DCl at 90 K with the $D_2O$/acid ratios increasing from top to bottom as indicated by labels. The vertical arrows mark the approximate amplitudes of the Zundel continua. The absorbance scale refers only to the 6:1 deuterate.

A substantial continuum contribution is reproducibly present even in the 50−60 K surface spectra of $DCl/D_2O$, underlying the *molecular* bands (Figure 12). (For HBr the low *T* continuum is much weaker, being close to the baseline error limit of 0.001 absorbance units.) The source of this low *T* continuum is uncertain. It may indicate DCl ionization to the Zundel form at an ~30% level as compared to the 90 K spectrum. However, the absence of concurrent *ionic* bands appears to contradict this suggestion. Another possible source is the Zundel effect from partial proton transfer from DCl to water molecules, in "nearly triply-coordinated" acid configurations, as in Figure 6k. At the 30% dose level, some acid molecules may acquire already at 60 K three, albeit stretched, hydrogen bonds, resulting in proton sharing configurations between water and chloride.

A third possibility is a generalized *molecular* Zundel effect, in which DCl/HCl remains mostly undissociated at 60 K; and the continuum absorption originates from static/dynamic fluctuations in molecular DCl/HCl environments, ranging from singly to "nearly triply" coordinated, as in Figure 6k. The discrete molecular bands, as seen in the 60 K spectra, would then correspond to a fraction of preferentially populated singly and doubly coordinated configurations. In this context one may note recent studies of the matrix-isolated $HCl\cdots NH_3$ dimer, in which the HCl frequency *shift* varied from −802 to −1515 and −1668 $cm^{-1}$ in the Ne, Ar, and Kr matrixes, respectively.[90] Although ammonia is a stronger proton acceptor than water, the extreme sensitivity of the acid frequency to the environment

may be valid for the HCl−ice system as well. Moreover, ab initio studies of HCl−water clusters (section 2.1) yielded essentially barrierless transitions between nearly isoenergetic but distinct bonding configurations, which correspond to different normal frequencies (see pairs of configurations (j) and (k), (i) and (o) in Figure 6.)

### 5. Summary: Evolution of the Acid−Adsorbate State on Ice Nanocrystals as a Function of Temperature

It is shown that cold ice nanoparticle surfaces provide a unique "micro-laboratory" for observation of progressive solvation stages of HCl. The main result of this study is spectroscopic identification of distinct states of HCl solvation in the 50−110 K range, including slightly stretched molecules, strongly distorted molecules on the verge of ionization, hydronium ions in contact with $Cl^-$, and, finally, an ionic surface phase rich in Zundel ions.

Three tools were applied to investigate acid−adsorbate states on ice nanoparticles: spectroscopic studies, MC simulations of molecular acid on an ice particle at 50 K, and ab initio calculations for water−acid clusters, with different choices of HCl coordinations. Each of these tools of itself is limited. The MC simulation does not allow for acid bond stretching or ionization upon solvation. Ab initio calculations on $(H_2O)_n$-$(HCl)_m$, $n = 7$, $m = 1, 2$ include bond stretching and ionization but are confined to limited dimensionality; moreover, the use of harmonic normal-mode analysis in these strongly anharmonic systems is problematic. The measured spectroscopic bands of the complex acid−nanoparticle system are broad and thus representative of a distribution of diverse adsorbate sites and configurations, which may be difficult to identify. Still, the combined information from the three sources seems to yield a reasonably consistent zero-order picture of the evolution of the system with temperature.

At low *T*, two broad bands were observed experimentally (Figure 8), downshifted by ∼400 and 1200 $cm^{-1}$ with respect to the gas phase of HCl. MC simulations of molecular HCl adsorbed on an ice particle suggest that the bands originate from singly and doubly coordinated HCl. Typical adsorbate configurations obtained in MC include d-O···HCl, d-O···HCl···d-H, and d-O···HCl···HCl. (The notation d-O/d-H is used for dangling water atoms, with unsaturated hydrogen bond coordination with respect to other $H_2O$. Additional nonspecific interactions of HCl, with surrounding acid and water molecules, are present.) Ab initio calculations for cluster models with singly and doubly coordinated HCl confirm that such HCl remains molecular. The low coordination of the molecular adsorbate on cold particles is ascribed to the low density of d-O and d-H-atoms on the ice surface that are available for adsorbate bonding. Ab initio frequency shifts calculated for singly and doubly coordinated HCl in cluster models (i) and (j) (Figure 6) are in fact close to those of the first and second measured bands, respectively. According to ab initio results, the Cl side of an HCl molecule can be solvated by another HCl nearly as well as by $H_2O$. Ab initio calculations suggest an additional contribution to the first observed band from such HCl molecules solvating the Cl side of the stretched HCl.

Substantial stretching of HCl in a doubly coordinated configuration is obtained only if the d-O molecule *does not have an additional acceptor bond from a water molecule*. This extra acceptor bond interferes with proton transfer, as shown in past studies of proton transfer in liquid water.[51−54] Because strongly stretched HCl molecules are observed already at 50 K, the molecular adsorbate appears to modify the ice particle surface beyond the results of the (rigid body) MC simulations, by eliminating the acceptor bonds of d-O molecules. Elimination of the interfering acceptor bonds is likely to be promoted by strengthening of the remaining hydrogen bonds as a result of HCl stretching and polarization. (Because the hydronium ion is triply coordinated,[91] the interfering bond must break on the way to the ionized state.)

Heating above 60 K is associated with gradual growth of ion bands. Spectroscopic features were identified due to $D_3O^+$ ions in contact with $Cl^-$, and DCl solvating $Cl^-$ (Figure 9). This assignment was made with the help of ab initio calculations for ionized cluster models with contact ion pairs (Figure 6m,n), and strengthened by the presence of the corresponding bands in the spectrum of the amorphous monodeuterate solid; the latter solid is rich in contact ions and is expected to include some acid self-solvation; see Appendix I. Ab initio calculations presented in section 2.1, as well as past electronic structure investigations,[7,9,11,44] indicate that acid ionization requires three hydrogen bonds. An increase in the observed contact-ion signal between 60 and 80 K suggests activated acquisition of a third hydrogen bond by the stretched doubly coordinated adsorbate molecules; the possible mechanisms include thermal cleaving of strained hydrogen bonds on the acid surface, and/or adsorbate self-solvation following HCl diffusion. The latter mechanism is supported by the observation of the $Cl^-$···HCl band. Spectroscopic evidence for $Cl^-$ solvation by other acid molecules is also consistent with the experimentally observed enhancement of ionization by high acid coverage.

A structural transition to an ionic surface phase rich in Zundel ions, is observed in the 90−100 K range at coverages ≥20% (Figures 9−11). An abundance of Zundel ions ($H_2O$···$H^+$···$OH_2$ and isotopic variants) is evidenced by a strong continuum absorption underlying the spectrum.[57] Formation of Zundel ions corresponds to one more stage of ionization: removal of the proton (or the deuteron) away from chloride, to a position between two water molecules. At the ∼20% coverage, the transition occurs relatively abruptly near 95 K, over a range of a few degrees. The spectrum of the resulting surface layer matches that of an amorphous hydrate (deuterate) solid, with an acid-to-water ratio in the 1:2 to 1:4 range, depending on the system. Higher dosage levels (≥30%) are accompanied by significant ionization already in the 50−90 K range, but a large jump is still observed in the ion signal near 90 K. Low acid dose levels <20% are associated with a gradual increase in the ion signal without a burst of ionization.

It should be emphasized that formation of the ion layer at ≥20% coverage should be viewed as nucleation of a new surface phase, rather than as dissolution of acid in ice. In contrast to liquid water, ice is a poor solvent of isolated molecules.[63] However, mixed solid phases of acid hydrates are readily formed at sufficiently high temperatures. As shown in past studies, extended exposure of ice to HCl at temperatures above 110 K results in propagation of the ionic hydrate phase into the ice interior.[21,25,30,32,33]

Our understanding of the acid adsorbate−ice nanoparticle system is still far from complete. One question pertains to the source of the continuum absorption underlying the *molecular* bands of DCl at 60 K (Figure 12; a similar continuum was observed for HCl). A possible source of the continuum is a "molecular Zundel effect", analogous to the ionic one, due to static and dynamic fluctuations in stretched molecular HCl environments (see section 4.3). Other open issues include molecular mechanisms of various processes occurring on the surface, such as elimination of acceptor bonds that interfere with

solvation, acquisition of a third hydrogen bond by doubly coordinated molecular HCl (which is necessary for $H_3O^+\cdots Cl^-$ contact-ion formation), and proton transfer, away from chloride to a position between two water molecules, during Zundel-ion formation. Perhaps the most exciting question is the mechanism of the *collective transition* near 95 K from a largely molecular adsorbate layer to an ionized one. The structure of the resulting ionized surface layer is also of interest; e.g., do factors other than acid concentration determine whether a dihydrate-like or a tetrahydrate-like structure is obtained? Another problem pertains to the band versus continuum contributions to the spectra. Do bands originate from "special" configurations, or from specific categories of motion? Is the continuum dominated by static or dynamic fluctuations in proton environments? What is the spatial range of excitations contributing to the very intense continuum? (An interesting possibility is proton dislocation over a whole range of bonding configurations during the excitation.)

Detailed modeling of the acid−surface system, including ionization and evolution of the spectra, would be a formidable task. A quantum (or at least semiclassical) treatment is required of nuclear motion in this cold, strongly anharmonic, and hydrogen-rich many-body system.[92] Lack of an accurate ionizing potential surface is another serious difficulty. The currently employed highest-level on-the-flight simulations are DFT-based. Tests of DFT (B3LYP version) for acid−water clusters indicate overestimation of the tendency of HCl to stretch and ionize (see refs 8 and 9 and section 2.2); therefore, applications to studies of transition from a molecular to an ionic adsorbate state are problematic. An accurate empirical potential for ionizing HCl is not available, to the best of our knowledge, but an extension of an ionizing water potential of ref 93 to include HCl is a possibility. Another promising approach would be an extension of the empirical valence bond scheme, which has been used successfully for proton transfer in water.[54,55]

**Acknowledgment.** Support by the National Science Foundation, Grant 9983185, KBN 7 T09A 111 21, and the Binational Science Foundation, Grant 9800208 is gratefully acknowledged. We also acknowledge, with thanks, the access of N.A-U. to computer services of the group of Prof. Donald Thompson.

**Supporting Information Available:** Appendix II, Figure S1, and Table SI containing additional information on MC simulations. This material is available free of charge via the Internet at http://pubs.acs.org.

## Appendix I: Thin-Film Hydrate and Deuterate Spectra

To interpret adsorbate spectra, one must be able to distinguish features due to molecular and ionic states. In fact, in the high temperature limit, adsorbate spectra approach those of the (ionic) hydrates. Therefore, HCl hydrate and deuterate spectra are discussed below.

Spectra of thin films of the amorphous and crystalline acid hydrates have been published along with tentative band assignments.[15,94] We follow the results of ref 15, but modified by the suggestion of Banham et al.[20] that, from the X-ray results,[58] the spectrum attributed to the crystalline tetrahydrate should be assigned to the trihydrate. Here, additional spectra of vapor-deposited films of DCl deuterates are reported. The spectra, which resemble the corresponding hydrate spectra moved to lower frequencies by mass effects modified by anharmonicity, are presented in Figures 13 and 14 for the amorphous and crystalline deuterates, respectively. The acid-to-water ratios range from 1:1 to 1:6.

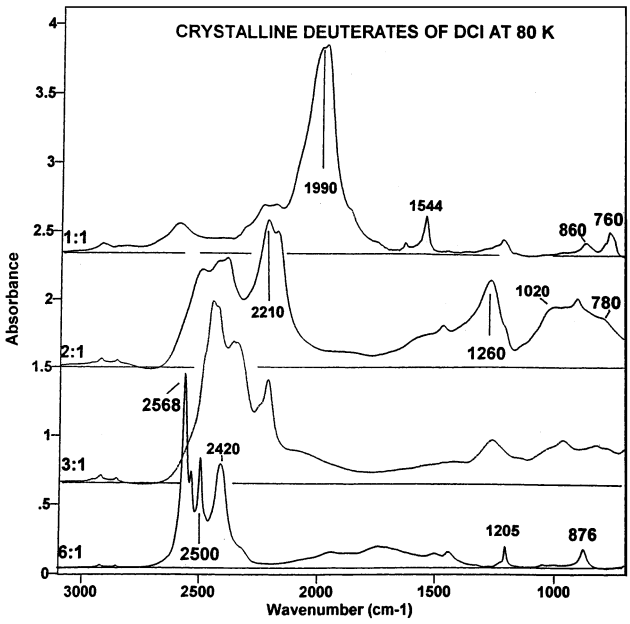


**Figure 14.** Infrared transmission spectra of crystalline deuterate films of DCl at 90 K.

The solids are largely ionic and include $Cl^-$ anions and protonated water cations. In crystalline hydrates a well-defined cation (either Zundel or hydronium) can be found, depending on the composition. On the basis of X-ray determinations of structures, the following formulas were proposed for HCl hydrates:[58] for the monohydrate, $(H_3O^+)(Cl^-)$; for the dihydrate, $(H_5O_2^+)(Cl^-)$; for the trihydrate, $(H_5O_2^+)(H_2O)(Cl^-)$; and for the hexahydrate, $(H_9O_4^+)(H_2O)_2(Cl^-)$ (the cation in this structure corresponds to an Eigen form, i.e., a hydronium cation fully solvated by three water molecules). Thus spectra of the hydronium and Zundel ions (solvated by $Cl^-$) can be seen in the spectra of crystal mono- and dihydrates (ref 15, Figure 2b,c) and mono- and dideuterates (Figure 14, top). As seen in Figure 14, the spectra of the crystal di- and trideuterates display an underlying continuum, which is a well-known signature of the Zundel ion.[57]

In amorphous hydrates and deuterates, and also on the ice nanoparticle surface, one can reasonably expect a continuum of proton configurations, ranging from hydronium to Zundel, in varying proportions. All amorphous solid spectra display the Zundel effect (Figure 13). A frozen distribution of ionic configurations is expected to contribute to the continuum, in addition to the dynamic modulation of the proton force field in the Zundel-like ions (see section 1). In the amorphous di-, tetra-, and hexadeuterate, the continuum constitutes most of the absorption intensity at frequencies below the OD stretch. Distinct features superimposed on the continuum originate from water molecules and also from ions, both hydronium and Zundel. (From the crystal dideuterate spectra in Figure 14 it is evident that the Zundel ion contributes distinct peaks, not only the continua.) The features observed in the *amorphous* hydrate/deuterate spectra will be used to probe ionized adsorbate states and are therefore discussed in more detail below.

The initial stage of adsorbate ionization in low dosage samples corresponds to formation of contact ion pairs, solvated by surrounding molecules. Spectroscopic signatures originating from contact ion pairs are therefore needed. Such features are expected to appear in mono- and dihydrate (deuterate) spectra, although in these solids, a cation is likely to be in contact with more than one anion. Amorphous mono- and dideuterates have five well-defined bands, at 2400, 2000, 1560, 1260, and near

800 $cm^{-1}$, corresponding to bands of the respective hydrates at 3144, 2548, 2110, 1686, and 1030 $cm^{-1}$.[15]

The broad band around 2548 (2000) $cm^{-1}$ in amorphous mono- and dihydrates (deuterates) is assigned to the bond-stretch vibration of cations in contact with $Cl^-$. Comparison to crystal spectra suggests that the low frequency wing of this band is dominated by $H_3O^+$ ($D_3O^+$), and the high frequency region by Zundel ions (because $D_3O^+$ cations in crystal monodeuterate absorb at lower frequencies than Zundel cations in crystal dideuterate; see Figure 14). The high frequency peak of the amorphous mono- and dihydrate (deuterate) stretch feature, near ~3144 (2400) $cm^{-1}$ should include contributions from (a) water, (b) the high frequency part of the stretch doublet of Zundel ions, as seen in the crystal dideuterate spectrum, and (c) the hydronium ion stretch of OH (OD), such that H (D) is in contact with water rather than with an anion. These assignments of the two amorphous hydrate (deuterate) stretch features are also supported by calculated spectra of cluster structures (m) and (n), which include hydronium and $Cl^-$ contact ion pairs (Figure 6). As seen in their ab initio spectra (Figure 7), the OH stretch transitions of the hydronium appear to the red from the water OH stretch, in the 3032−2292 $cm^{-1}$ frequency range; the lowest frequency vibration corresponds to OH in contact with the anion.

A second spectral feature characteristic of amorphous mono- and dihydrates (deuterates) and also of the adsorbate−surface systems, is observed at 2110 (1560) $cm^{-1}$. This band is assigned to a stretch vibration of HCl (DCl) molecules solvating $Cl^-$. A corresponding high intensity transition was computed for $Cl^-\cdots HCl$ in structure (n) at 2121 $cm^{-1}$. The $Cl^-\cdots HCl$ species was also reported by Laasonen and Klein in an ab initio molecular dynamics study of a concentrated aqueous HCl solution.[95]

The band observed in amorphous mono- and dihydrates (deuterates) at 1686 (1260) $cm^{-1}$ has a computed counterpart at a similar frequency, originating from a combination of water and $H_3O^+$ bending (Figure 7). Although our ab initio models do not include Zundel ions,[96] inspection of crystal dihydrate and dideuterate spectra suggests that the latter undergo a bending excitation in this region as well. The computed features at ~1400 and ~1000 $cm^{-1}$ (Figure 7) correspond, respectively, to $H_3O^+$ umbrella bending, and libration (with contributions from both $H_2O$ and $H_3O^+$). Experimentally, a single broad peak is observed in the 1030 (800) $cm^{-1}$ region for amorphous mono- and dihydrate (deuterate). On the basis of the computations, the high and low frequency end of this feature is tentatively assigned to contributions from cation bending, and from libration.

In higher amorphous hydrates, the 2548 (2000) and 2110 (1560) $cm^{-1}$ features disappear, in accord with their respective assignment to the OH (OD) stretch in contact ions, and to the HCl (DCl) stretch in $Cl^{-1}\cdots HCl$ ($Cl^{-1}\cdots DCl$). At high water-to-acid ratios, all acid is likely to be ionized and solvated by water, making improbable the contact ions and the $Cl^{-1}\cdots HCl$ configurations. A single OH (OD) stretch feature is visible at 3200 (2500) $cm^{-1}$, which most likely includes both water and cation contributions. An *apparent* discrepancy is obtained with the calculated spectrum of structure (l) in Figure 6, in which the ion pair is separated by water. The calculated spectrum (Figure 7, top) includes one intense low frequency feature at 2059 $cm^{-1}$, which is absent in the experimental spectra, and which originates from the longest OH bond in the cation. As discussed in section 2.2, the $H_3O^+$ ion in this model is distorted toward the Zundel structure, and in an accurate anharmonic calculation of the spectrum the corresponding transition would most likely contribute to the continuum.

One may note finally the very large Zundel continuum intensity in the amorphous deuterate (and hydrate) spectra. In the hexadeuterate, similar integrated intensities were obtained for the OD stretch band above 2100 $cm^{-1}$, and for the continuum below 2100 $cm^{-1}$. However, there are 12 times as many D-oscillators that contribute to the OD-stretch band than deuterons. This result suggests an enhancement of the deuteron continuum intensity by an order of magnitude with respect to the already intense OD-stretch band. (The integrated stretch intensity is similar to that of an ice film of the same thickness.[97]) This argument is oversimplified because the continuum is most likely contributed by compound molecular motions rather than by vibrations of deuterons only.[54,55,57] The continuum intensity per deuteron, as measured at the frequency marked by an arrow in Figure 13, is in fact roughly proportional to the water-to-acid ratio, indicating collective vibrations involving water. Still, the pertinent motions appear to be "ïlluminated" by deuterons in Zundel-like configurations. This follows from the infrared absorption of $D_2O$ ice below 2100 $cm^{-1}$ being much weaker than that of the stretch band;[97] note also the weakness of the spectral features below 1800 $cm^{-1}$ in the crystal mono- and hexadeuterate, which include hydronium rather than Zundel cations (Figure 14).

## References and Notes

(1) Molina, M. J.; Tso, T. L.; Molina, L. T.; Wang, F. C. Y. *Science* **1987**, *238*, 1253.
(2) Tolbert, M. A.; Rossi, M. J.; Malhotra, R.; Golden, D. M. *Science* **1987**, *238*, 1258.
(3) Abbatt, J. P. D.; et al. *J. Geophys. Res.* **1992**, *97*, 15819.
(4) Amirand, C.; Maillard D. *J. Mol. Struct.* **1988**, *176*, 181.
(5) Packer, M. J.; Clary, D. C. *J. Phys. Chem.* **1995**, *99*, 14323.
(6) Planas, M.; Lee, C.; Novoa, J. *J. Phys. Chem.* **1996**, *100*, 16495.
(7) Re, S.; Osamura; Y.; Suzuki; Y.; Schaefer, H. F., III. *J. Chem. Phys.* **1998**, *109*, 978.
(8) Smith, A.; Vincent, M. A.; Hillier, I. H. *J. Phys. Chem. A* **1999**, *103*, 1132.
(9) Bacelo, D. E.; Binning, R. C.; Ishikawa, Y. *J. Phys. Chem. A* **1999**, *103*, 4631.
(10) Milet, A.; Struniewicz, C.; Moszynski, R.; Wormer, P. E. S. *J. Chem. Phys.* **2001**, *115*, 349.
(11) Chaban, G. M.; Gerber, R. B.; Janda, K. C. *J. Phys. Chem. A* **2001**, *105*, 8323.
(12) Conley, C.; Tao, F. M. *Chem. Phys. Lett.* **1999**, *301*, 29.
(13) Gertner, B. J.; Peslherbe, G. H.; Hynes, J. T. *Isr. J. Chem.* **1999**, *39*, 273.
(14) Hanson, D. R.; Ravishankara, A. R. *J. Phys. Chem.* **1992**, *96*, 2682, 9441.
(15) Delzeit, L.; Rowland, B.; Devlin, J. P. *J. Phys. Chem.* **1993**, *97*, 10312.
(16) Chu, L. T.; Leu, M. T.; Keyser, L. F. *J. Phys. Chem.* **1993**, *97*, 7779.
(17) Rieley, H.; Aslin, H. D.; Haq, S. J. *Chem. Soc. Faraday Trans.* **1995**, *91*, 2349.
(18) Banham, S. F.; Horn, A. B.; Koch, T. G.; Sodeau, J. R. *Faraday Discuss.* **1995**, *100*, 321.
(19) Graham, J. D.; Roberts, J. T. *J. Phys. Chem.* **1994**, *98*, 5974; *Geophys. Res. Lett.* **1995**, *22*, 251.
(20) Banham, S. F.; Sodeau, J. R.; Horn, A. B.; McCoustra, M. R. S.; Chesters, M. A. *J. Vac. Sci. Technol. A* **1996**, *14* (3), 1620.
(21) Delzeit, L.; Powell, K.; Uras, N.; Devlin, J. P. *J. Phys. Chem. B* **1997**, *101*, 2327.
(22) Foster, K. L.; Tolbert, M. A.; George, S. M. *J. Phys. Chem. A* **1997**, *101*, 4979.
(23) Donsig, H. A.; Vickerman, J. C. *J. Chem. Soc., Faraday Trans.* **1997**, *93*, 2755.
(24) Uras, N.; Rahman, M.; Devlin, J. P. *J. Phys. Chem. B* **1998**, *102*, 9375.
(25) Barone, S. B.; Zondlo, M. A.; Tolbert, M. A. *J. Phys. Chem. A* **1999**, *103*, 9717.
(26) Isakson, M. J.; Sitz, G. O. *J. Phys. Chem. A* **1999**, *103*, 2044.
(27) Andersson, P. U.; Nagard, M. B.; Pettersson, J. B. C. *J. Phys. Chem. B* **2000**, *104*, 1596.

(28) Kang, H.; Shin, T. H.; Park, S. C.; Kim, I. K.; Han, S. J. *J. Am. Chem. Soc*. **2000**, *122*, 9842.
(29) Sadtchenko, V.; Giese, C. F.; Gentry, W. R. *J. Phys. Chem. B* **2000**, *104*, 9421.
(30) Uras-Aytemiz, N.; Joyce, C.; Devlin, J. P. *J. Phys. Chem. A* **2001**, *105*, 10497.
(31) Demirdjian, B.; Ferry, D.; Suzanne, J.; Toubin, C.; Picaud, S.; Hoang, P. N. M.; Girardet, C. *J. Chem. Phys*. **2002**, *116*, 5143.
(32) Haq, S.; Harnett, J.; Hodgson, A. *J. Phys. Chem. B* **2002**, *106*, 3950.
(33) Hudson, P. K.; Foster, K. L.; Tolbert, M. A.; George, S. M.; Carlo, S. R.; Grassian, V. H. *J. Phys. Chem. A* **2001**, *105*, 694.
(34) Kroes, G. J.; Clary, D. C. *J. Phys. Chem.* **1992**, *96*, 7079.
(35) Robertson, S. H.; Clary, D. C. *Faraday Discuss.* **1995**, *100*, 309.
(36) Gertner, B. J.; Hynes, J. T. *Science* **1996**, *271*, 1563.
(37) Clary, D. C.; Wang, L. *J. Chem. Soc., Faraday Trans*. **1997**, *93*, 2763. Wang, L.; Clary, D. C. *J. Chem. Phys*. **1996**, *104*, 5663.
(38) Geiger, F. M.; Hicks, J. M.; de Dios, A. C. *J. Phys. Chem. A* **1998**, *102*, 1514.
(39) Gertner, B. J.; Hynes, J. T. *Faraday Discuss.* **1998**, *110*, 301.
(40) Bussolin, G.; Casassa, S.; Pisani, C.; Uglieno, P. *J. Chem. Phys*. **1998**, *108*, 9516.
(41) Al-Halabi, A.; Kley, A. W.; Kroes, G. J. *Chem. Phys. Lett*. **1999**, *307*, 505.
(42) Casassa, S. *Chem. Phys. Lett*. **2000**, *321*, 1.
(43) Allouche, A.; Couturier-Tamburelli, I.; Chiavassa, T. *J. Phys. Chem. B* **2000**, *104*, 1497.
(44) Svanberg, M.; Pettersson, J. B. C.; Bolton, K. J. *J. Phys. Chem. A* **2000**, *104*, 5787.
(45) Mantz, Y. A.; Geiger, F. M.; Molina, L. T.; Molina, M. J.; Trout, B. L. *J. Phys. Chem. A* **2001**, *105*, 7037
(46) Mantz, Y. A.; Geiger, F. M.; Molina, L. T.; Molina, M. J.; Trout, B. L. *Chem. Phys. Lett.* **2001**, *348*, 285.
(47) Toubin, C.; Picaud, S.; Hoang, P. N. M.; Girardet, C.; Demirdjian, B.; Ferry, D.; Suzanne, J. *J. Chem. Phys.* **2002**, *116*, 5150.
(48) Devlin, J. P.; Uras, N.; Sadlej, J.; Buch, V. *Nature* **2002**, *487*, 269.
(49) Elliot, S.; Turco, R. P.; Toon, O. B.; Hamill, P. J. *Atmos. Chem*. **1991**, *13*, 211. Hanson, D. R.; Mauersberger, K. *J. Chem. Phys.* **1990**, *94*, 4700.
(50) Tabazadeh, A.; Turco, R. P. J. *Geophys. Res.* **1993**, *98* (D7), 12727.
(51) Agmon, N. *Chem. Phys. Lett.* **1995**, *244*, 456.
(52) Ando, K.; Hynes, J. T. *J. Phys. Chem. B* **1997**, *101*, 10464.
(53) Tuckerman, M.; Laasonen, K.; Sprik, M.; Parrinello, M. *J. Chem. Phys.* **1995**, *103*, 150.
(54) Vuillemier, R.; Borgis, D. *J. Phys. Chem. B* **1998**, *102*, 4261; *J. Mol. Struct. 2000*, **117**, 552.
(55) Schmitt, U. W.; Voth, G. A. *J. Chem. Phys*. **1999**, 111, 9361. Kim, J.; Schmitt, U. W.; Gruetzmacher, J. A.; Voth, G. A.; Scherer, N. E. *J. Chem. Phys*. **2002**, *116*, 737.
(56) Marx D.; Tuckerman M. E.; Hutter J.; Parrinello M. *Nature* **1999**, *397*, 601.
(57) Zundel, G. *Adv. Chem. Phys*. **2000**, 111, 1.
(58) (a) Monohydrate: Yoon, Y. K.; Carpenter, G. B. *Acta Crystallogr*. **1959**, *12*, 17. (b) Dihydrate: Lundgren, J. O.; Olovsson, I. *Acta Crystallogr*. **1967**, *23*, 966. (c) Trihydrate: Lundgren, J. O.; Olovsson, I. *Acta Crystallogr*. **1967**, *23*, 971. (d) Hexahydrate: Taesler, I.; Lundgren, J. O. *Acta Crystallogr*. **1978**, *B34*, 2424.
(59) Cotton, F. A.; Wilkinson, G. *Advanced Inorganic Chemistry*; Wiley: New York, 1980; p 231.
(60) Heerman, D. W. *Computer Simulation Methods in Theoretical Physics*; Springer-Verlag: Berlin, 1986.
(61) Uras, N.; Buch, V.; Devlin, J. P. *J. Phys. Chem. B* **2000**, *104*, 9203.
(62) Hobbs, P. V. *Ice Physics*; Clarendon: Oxford, U.K., 1974.
(63) Petrenko, V. F.; Whitworth, R. W. *Physics of Ice*; Oxford University Press: Oxford, U.K., 1999.
(64) Torchet, G.; Schwartz, P.; Farges, J.; de Feraudy, M. F.; Raoult, B. *J. Chem. Phys.* **1983**, *79*, 6196
(65) Bartell, L. S.; Huang, J. *J. Phys. Chem***. 1994**, *98*, 7455. Huang, J.; Bartell, L. S. *J. Phys. Chem*. **1995**, *99*, 3924.
(66) (a) Rowland, B.; Kadagathur N. S.; Devlin, J. P. *J. Chem. Phys.* **1995**, *102*, 13. (b) Buch, V.; Delzeit, L.; Blackledge, C.; Devlin, J. P. *J. Phys. Chem*. **1996**, *100*, 10076.
(67) Reviews: Devlin, J. P.; Buch, V. *J. Phys. Chem*. **1995**, *99*, 16534; **1997**, *101*, 6095.
(68) Delzeit, L.; Devlin, M. S.; Rowland, B.; Devlin, J. P.; Buch, V. *J. Phys. Chem*. **1996**, *100*, 10076. Delzeit, L.; Devlin, J. P.; Buch, V. *J. Chem. Phys*. **1997**, *107*, 3726.
(69) (a) Devlin, J. P.; Joyce, C.; Buch, V. *J. Phys. Chem. A* **2000**, *104*, 1974. (b) Devlin, J. P.; Sadlej, J.; Buch, V. *J. Phys. Chem. A* **2001**, *105*, 974.
(70) Buch, V.; Sandler, P.; Sadlej, J. *J. Phys. Chem. B* **1998**, *102*, 8641.
(71) Jorgensen, W. L.; Chandrasekhar, J.; Madura, J. D.; Impey, R. W.; Klein, M. L. *J. Chem. Phys.* **1983**, *79*, 926.
(72) Votava, C.; Ahlrichs, R.; Geiger, A. *J. Chem. Phys*. **1983**, *78*, 6841.
(73) Meredith, A. W.; Ming, L.; Nordholm, S. *Chem. Phys.* **1997**, *220*, 63.
(74) Bacskay, G. B. *Mol. Phys*. **1992**, *77*, 61
(75) Goldstein, H. *Classical Mechanics*; Addison-Wesley: Reading, MA. 1980.
(76) Dunning, T. H. *J. Chem. Phys*. **1989**, *90*, 1007.
(77) Frisch, M. J.; Trucks, G. W.; Schlegel, H. B.; Scuseria, G. E.; Robb, M. A.; Cheeseman, J. R.; Zakrzewski, V. G.; Montgomery, J. A., Jr.; Stratmann, R. E.; Burant, J. C.; Dapprich, S.; Millam, J. M.; Daniels, A. D.; Kudin, K. N.; Strain, M. C.; Farkas, O.; Tomasi, J.; Barone, V.; Cossi, M.; Cammi, R.; Mennucci, B.; Pomelli, C.; Adamo, C.; Clifford, S.; Ochterski, J.; Petersson, G. A.; Ayala, P. Y.; Cui, Q.; Morokuma, K.; Malick, D. K.; Rabuck, A. D.; Raghavachari, K.; Foresman, J. B.; Cioslowski, J.; Ortiz, J. V.; Stefanov, B. B.; Liu, G.; Liashenko, A.; Piskorz, P.; Komaromi, I.; Gomperts, R.; Martin, R. L.; Fox, D. J.; Keith, T.; Al-Laham, M. A.; Peng, C. Y.; Nanayakkara, A.; Gonzalez, C.; Challacombe, M.; Gill, P. M. W.; Johnson, B. G.; Chen, W.; Wong, M. W.; Andres, J. L.; Head-Gordon, M.; Replogle, E. S.; Pople, J. A. *Gaussian 98*, revision x.x; Gaussian, Inc.: Pittsburgh, PA, 1998.
(78) Xantheas, S. S.; Dunning, T. H. *J. Chem. Phys*. **1993**, *99*, 8774. Xantheas, S. S. *J. Chem. Phys.* **1994**, *100*, 7523.
(79) Huber, K. P.; Herzberg, G. *Molecular Spectra and Molecular Structure IV, Constants of Diatomic Molecules*; Van Nostrand Reinhold: New York, 1979.
(80) Benedict, W. S.; Gailar, N.; Plyler, E. K. *J. Chem. Phys*. **1956**, *24*, 1139.
(81) Boys, S. F.; Bernardi, F. *Mol. Phys.* **1970**, *19*, 553.
(82) Huisken, F.; Kaloudis, M.; Kulcke, A. *J. Chem. Phys.* **1996**, *104*, 17.
(83) Liu, K.; et al. *Nature* **1996**. *381*, 501.
(84) Brudermann, J.; et al. *J. Chem. Phys*. **1999**, *110*, 10649.
(85) We did not succeed in constructing a three-dimensional cluster model with a bridge configuration d-O···HCl···HCl, which is stable with respect to ab initio minimization. Efforts to construct such models were made following MC results for the higher coverage.
(86) Delzeit, L.; Blake, D. *J. Geophys. Res.-Planets* **2001**, 106, 33371.
(87) Nakamoto, K. *Infrared Spectra of Inorganic and Coordination Compounds*; Wiley: New York, 1963.
(88) Warshel, A. *Computer Modeling of Chemical Reactions in Enzymes and Solutions*; Wiley: New York, 1991.
(89) Severson, M.; Buch, V.; Rusted, J. Manuscript in preparation.
(90) Andrews, L.; Wang, X.; Mielke, Z. *J. Phys. Chem. A* **2001**, *105*, 6054.
(91) Kobayashi, C.; Saito, S.; Ohmine, I. *J. Chem. Phys*. **2000**, *113*, 9090.
(92) Von Rosenvinge, T.; Tuckerman, M. E.; Klein, M. L. *Faraday Discuss.* **1997**, *106*, 273.
(93) Halley, J. W.; Rustad, J. R. *J. Chem. Phys.* **1993**, *98*, 4110.
(94) Gilbert, A. S.; Sheppard, N. J. *Chem. Soc., Faraday Trans*. **1973**, *69*, 1628.
(95) Laasonen, K. E.; Klein, M. L. *J. Phys. Chem. A* **1997**, *101*, 98.
(96) We did not attempt ab initio studies of clusters with Zundel cations, because the value of normal-mode analysis in these strongly anharmonic systems is questionable.
(97) Bertie, J. E.; Labbe, J.; Whalley, E. *J. Chem. Phys*. **1969**, *50*, 4501.